Altered synaptic adaptation and gain in sensory circuits of the casein kinase 1 delta ($CK1d_{T44A}$) mouse model of migraine

Pratyush Suryavanshi[1], Punam Sawant Pokam[1], KC Brennan[1]

[1]Neurology, University of Utah, Salt Lake City, United States

Abstract

Migraine is a very common and disabling neurological disorder that remains poorly understood at the cellular and circuit level. Transgenic mice harboring a mutation in casein kinase 1 delta ($CK1d_{T44A}$) represent the first animal model of non-hemiplegic migraine. These mice have decreased sensory thresholds to mechanical and thermal pain after treatment with the migraine trigger nitroglycerin; and an increased susceptibility to cortical spreading depression (CSD), which models the migraine aura. In this study, we investigated cellular and synaptic mechanisms within sensory cortical circuits that might underlie the migraine relevant phenotypes of $CK1d_{T44A}$ mice, using *in vitro* and *in vivo* whole cell electrophysiology. Surprisingly we found that at resting state, $CK1d_{T44A}$ neurons exhibited hyperpolarized membrane potentials, due to increased tonic inhibition. Despite this reduction in baseline excitability, $CK1d_{T44A}$ neurons fired action potentials more frequently in response to current injection. And despite similar synaptic and dendritic characteristics to wild type neurons, excitatory but not inhibitory $CK1d_{T44A}$ synapses failed to adapt to high frequency short-stimulus trains, resulting in elevated steady state excitatory currents. The increased steady state currents were attributable to an increased replenishment rate of the readily releasable pool, providing a presynaptic mechanism for the $CK1d_{T44A}$ phenotype. Finally, during *in vivo* experiments, $CK1d_{T44A}$ animals showed increased duration and membrane potential variance at 'cortical up states', showing that the intrinsic and synaptic changes we observed have excitatory consequences at the local network level. In conclusion excitatory sensory cortical neurons and networks in $CK1d_{T44A}$ animals appear to exhibit decreased adaptation and increased gain that may inform the migraine phenotype.

Introduction

Migraine affects 12% of the world population[1], and causes enormous disability, especially to women and to those in working and childbearing years[2,3]. Yet the disease remains poorly understood at the cellular and circuit level. Although migraine is typically associated with headache, multiple lines of evidence suggest it is a more widespread disorder of multisensory excitability and sensory gain of function[4]. Migraine attacks involve amplifications of multiple sensory inputs including light, sound, smell, touch, and interoception (photophobia, phonophobia, osmophobia, allodynia, and nausea, respectively)[5,6]. For one third of migraine patients the attack is preceded by an aura, mediated by a massive spreading depolarization of cortical tissue[7]. Finally, both migraine models and migraine patients exhibit a blunted response to repetitive sensory stimulation[8,9].

However, the circuit mechanisms underlying this increased network excitability are essentially unknown. In this regard transgenic mouse models can be helpful[10]. Mutations found in familial hemiplegic migraine, a severe and rare form of the disease, show increases in neuronal excitability that are consistent with the network phenotypes[11,12]. Recently a new monogenic migraine mutation was identified, in two families carrying a loss of function mutation in casein kinase 1 delta ($CK1d_{T44A}$)[13]. Though the $CK1d_{T44A}$ mutation is also rare, in contrast to prior mutations, $CK1d_{T44A}$ mutations segregated with phenotypically normal, non-hemiplegic migraine. Thus it is possible that insights gained from the model might be of broad relevance to the disease. Mice carrying a $CK1d_{T44A}$mutation had increased sensitivity to nitroglycerin (NTG), which induces migraine in humans with the disease. They also had an increased susceptibility to CSD[13]. Both NTG and CSD results provide face validity regarding migraine relevance, and are consistent with an excitable network[13]. However unlike other monogenic migraine mutations, which encode proteins of obvious relevance to excitability, the $CK1d_{T44A}$mutation is in a ubiquitous serine threonine kinase with broad roles across the organism[14–17]. Thus it is important to establish the cellular and circuit mechanisms that underlie the migraine phenotype of $CK1d_{T44A}$mice.

Abbreviations

APs: action potentials, AHP: After-hyperpolarizaion, CSD: cortical spreading depression, CK1d: Casein kinase 1 delta, RRP: Readily releasable pool, PPR: Paired pulse ratio, V_m: resting membrane potential, R_m: membrane resistance, F/I curve: Frequency-current curve, I/O curve: input-output curve, IV curve: current-voltage curve, HCN channels: hyperpolarization activated cyclic nucleotide gated channels, I_h currents: Hyperpolarization induced currents, AMAPRs: α-amino-3-hydroxy-5-methyl-4-isoxazolepropionic acid receptors, NMDARs: N-methyl-D-aspartic acid receptors, GABA: gamma-aminobutericacid E/IPSCs: Excitatory/Inhibitory post synaptic currents, TTX: tetrodotoxin, PTX: picrotoxin, L2/3 or 4 or 5_a: cortical layer 2/3 or 4 or or 5_a, S1: primary somatosensory cortex

Methods

Animal care and handling

All protocols were approved by the Institutional Animal Care and Use Committee at the University of Utah. Animals were housed in temperature-controlled room on a 12-hour light-dark cycle. Experimenters were blind to the genotypes in all experiments.

In vitro brain slice preparation

$CK1d_{T44A}$ and wild type (WT) littermate mice (males, 2-3 months old) were deeply anesthetized with 4% isoflurane, and the brain removed for slice preparation. Coronal sections were cut in ice cold dissection buffer (in mM; 220 Sucrose, 3 KCl, 10 $MgSO_4$, 1.25 NaH_2PO_4, 25 $NaHCO_3$, 25 Glucose, 1.3 $CaCl_2$), Sections containing somatosensory cortex[18] were allowed to recover in a chamber normal artificial cerebrospinal fluid (ACSF: in mM; 125 NaCl, 3 KCl, 10 $MgSO_4$, 1.25 NaH_2PO_4, 25 $NaHCO_3$, 25 Glucose, 1.3 $CaCl_2$, and saturated with 95%O_2 / 5%CO_2) at 35°C. For electrophysiology experiments, the sections were transferred to a submerged chamber constantly supplied with ACSF (flow rate: 2.5 mL/min, saturated with 95%O_2 / 5%CO_2) also maintained at 35°C.

In vitro Electrophysiology recordings

All whole-cell patch clamp recordings were obtained from regular spiking pyramidal neurons[18] in L2/3 somatosensory cortex. Neurons were visualized using differential interference contrast (DIC) microscopy and patched using glass microelectrodes (4-6 MΩ resistance, tip size of 3-4 µm). To record intrinsic membrane properties, patch electrodes were filled with intracellular solution containing 135 K-gluconate, 8 NaCl, 5 EGTA, 10 HEPES, 0.3 GTP, 2 ATP, 7 phosphocreatine (concentrations in mM, pH = 7.2). Baseline membrane voltage (resting membrane potential or Vm) as well as membrane voltage responses to 20 pA current injections steps (from -100 to 400pA) were recorded. Spontaneous excitatory and inhibitory post synaptic currents (EPSCs/IPSCs) were recorded using patch pipette containing 130 CsMeSO4, 3 CsCl, 10 HEPES, 2 MgATP, 0.3 Na3GTP, 5 EGTA, 10 Phosphocreatine, 5 QX-314, 8 biocytin (Concentration in mM; pH 7.3). Excitatory and inhibitory currents were isolated by clamping neuronal membrane potential to -70mV (inhibitory reversal potential) and 10mV (excitatory reversal potential) respectively. EPSCs and IPSCs were pharmacologically blocked by DNQX (50 µM) and picrotoxin (20 µM) respectively; confirming the AMPA and $GABA_a$ receptor mediated nature of the respective currents.

Recording AMPA/NMDA ratio

For AMPA/NMDA ratio measurements, a concentric bipolar metal stimulating electrode (AM systems, tip diameter ~75µm) connected to a stimulus isolator (World Precision Instruments) was placed on L4 and L5a (~400µm distance from recording site). Post-synaptic evoked AMPA and NMDA receptor mediated currents were recorded by stimulating L4 and $L5_a$ (1ms, 1 to 10mV stimuli). Stimulation intensity providing ~50% of maximum response with no failure was selected for further experiments. Evoked AMPA currents were isolated at -70mV. Evoked NMDA mediated currents were isolated at 40mV in presence of DNQX (50 µM) and picrotoxin (20 µM).[19]

Tonic inhibitory current recording

Tonic inhibitory current was pharmacolocally isolated using nonspecific $GABA_A$ receptor inhibitor 20 µM picrotoxin (PTX) for at least 10 mins. PTX application reduced both tonic as well as phasic inhibitory current, evident by narrowing of current data point (pA) distribution. in Tonic current was measured by subtracting inhibitory holding currents recorded (at 10 mV) after picrotoxin treatment from baseline holding current.

Recording HCN channel mediated I_h current

To record HCN mediated (I_h) currents, neurons were patched using a cesium based internal solution (see above). Slices were perfused in ACSF containing in µM: 0.75 TTX, 10 NBQX (2,3-dihydroxy-6-nitro-7-sulfamoyl-benzo[f]quinoxaline-2,3-dione), 10 gabazine, 5 CPP (3-[2-carboxypiperazin-4-yl]-propyl-1-phosphonic acid), and 3mM tetraethylammonium chloride to ensure blockade of most voltage gated and leak currents. Hyperpolarizing pulses (from -40mV to -100mV, 500ms) were applied to record 'control' inward currents. HCN mediated currents were isolated using the selective antagonist ZD7288 (25µM) and subtracting currents recorded in the presence of ZD7288 from control currents (ZD7288 sensitive currents)[20].

Stimulus train evoked E/IPSCs

For stimulus train experiments, bipolar stimulation electrodes were fabricated from pulled theta glass pipettes with 0.5 to 1GΩ resistance (4-7 µm tip diameter), and filled with saline. Chlorinated silver wires inserted into each half of the theta glass were connected to the two poles of the stimulus isolator. Distinct barrels in L4 somatosensory cortex were identified using IR-DIC microscopy[21]. Theta glass stimulation electrodes were placed at the bottom edge of the barrels. Postsynaptic L2/3 neurons from the same cortical column were patched for voltage clamp recording. Postsynaptic responses to 100 µs stimuli ranging from 1 to 10 mV intensity were recorded to establish input-output relationships. Range of stimulus intensity was restricted to evoke only column-specific monosynaptic EPSC and disynaptic IPSC responses. Stimulus intensity sufficient to evoke ~50% of the maximum responses was selected for the rest of the experiment. Trains of 10 or 30 stimuli were introduced at different frequencies (10/20/50 Hz) and resulting monosynaptic EPSC and disynaptic IPSC responses were measured by clamping post-synaptic cell voltage at -70mV and 10 mV respectively[22].

In vivo whole-cell recordings.

Mice (males; 2-3 months old) were anesthetized using urethane (0.75 g/kg; i.p.) supplemented with isoflurane (~0.5 %). Body temperature was monitored and maintained at 35 - 37°C using a heating pad. Vital signs (HR: 470–540 bpm, SpO2: 92-98%, respiration: 120-140/min) were monitored (MouseStat, Kent Scientific) throughout the experiment, and maintained within a physiologically normal range. An Omega-shaped head bar was mounted on the skull, using glue and dental cement, and affixed with screws to a holding rod attached to the stage. A craniotomy 2 mm in diameter was made above the hindpaw region of somatosensory cortex (1 mm caudal to the bregma and 2 mm lateral to the midline), and filled with 1.5% agarose (in ACSF) in order to keep the cortical surface moist and dampen the movement associated with breathing[18]. We used

in vivo whole-cell techniques to record the membrane potential from L2/3 neurons in the mouse somatosensory cortex and analyzed spontaneous up states in current-clamp mode at resting membrane potential (i.e., -65 to -70 mV). Patch electrodes with 4-6 MΩ resistance and longer taper were used (tip size of 3-4 µm)[18], filled with intracellular solution containing potassium gluconate to record membrane voltages and cesium methanesulphonate to record excitatory and inhibitory currents (see above).

Data analysis.

All whole cell recordings were acquired at 20kHz and filtered at 2kHz (lowpass) using Axopatch 700B amplifier. Analog data were digitized using Digidata 1330 digitizer and clampex 9 software (Axon Instruments). Access resistance was monitored throughout recordings (5mV pulses at 50Hz). Recordings with access resistance higher than 20 MΩ or with > 20% change in the access resistance were discarded from analysis. 70% series resistance compensation was applied to recorded currents in voltage clamp setting. Offline data processing was done with clmapfit 10 (Axon Instruments) and analysis was performed using GraphPad Prism 5 (GraphPad Software, San Diego, California), MATLAB 7.8.0 (Mathworks), Stata (statacorp) and Microsoft Excel (Microsoft Corp). Normality of distributions was determined using D'Agostino-Pearson K2 test. Average values for individual cells were compared across genotypes using student's t test (parametric data) or Mann Whitney U test (non-parametric data), whereas probability distributions of individual events were compared across genotype using two sample Kolmogorov–Smirnov (KS) test. For the analysis of current/voltage (IV curve), frequency/input current (F/I curve) relationships, and normalized post-synaptic currents in response to stimulus trains, comparisons across genotype for different values of input current/stimuli were made using two-way ANOVA (Kruskal Wallis test for non parametric data) with Bonferroni's post hoc test. To compare rise kinetics of IV and F/I curves, linear regression was fitted across datasets and slope were compared between genotypes. For the analysis of cumulative amplitudes of post-synaptic currents in response to stimulus trains, steady state responses were fitted with linear regression, and the initial fast rise was fitted with a single phase exponential[23,24]. For pharmacology experiments, comparisons between cells before and after drug treatment within a genotype were done by paired t-test; comparisons between control and drug treatment groups across genotypes were done by two-way ANOVA with Tukey's post hoc test. Data points more or less than 3 times standard deviation (parametric data) or mean standard error (non-parametric data) of the dataset were regarded as outliers.

Results:

Hyperpolarized membrane potential in CK1d$_{T44A}$ L2/3 pyramidal neurons due to increased tonic inhibition

To determine whether the migraine relevant excitable phenotype seen in CK1d$_{T44A}$mice *in vivo*[13] could be attributed to intrinsic membrane excitability of pyramidal neurons in sensory cortex, we performed whole cell current clamp experiments from L2/3 excitatory somatosensory cortical neurons. On the contrary, we found that resting membrane potentials (V_m) in CK1d$_{T44A}$ neurons were significantly hyperpolarized compared to those of WT neurons (figure 1C, $p<0.05$, Mann Whitney test; WT n=21 neurons and CK1d$_{T44A}$ n=22 neurons). Membrane resistance (R_m) which dictates V_m responses to subthreshold current injections, was not different between the two genotypes when calculated as slope of I/V curve (figure 1D, p=0.99, ANCOVA) or R_m values for individual neurons (figure 1E, p=0.36, Mann Whitney test, WT n=21, CK1d$_{T44A}$ n=22); suggesting no difference in intrinsic membrane excitability. Therefore, instead of hyperexcitability, CK1d$_{T44A}$ were found to be hypoexcitable at resting state.

A candidate mechanism for resting state hyperpolarization is tonic inhibitory currents[25]. We pharmacologically isolated tonic inhibitory currents using the $GABA_A$ receptor antagonist picrotoxin (20 µM) in CK1d$_{T44A}$ and WT neurons. We found that CK1d$_{T44A}$ neurons had significantly larger tonic inhibitory currents compared to WT (figure 1G, p=0.03, Mann Whitney test, WT n=8, CK1d$_{T44A}$ n=8). To determine if increased tonic inhibitory currents in CK1d$_{T44A}$ neurons resulted in hyperpolarization, we recorded resting V_m before and after picrotoxin treatment. Though V_m in both WT and CK1d$_{T44A}$ neurons was depolarized following picrotoxin treatment, depolarization in CK1d$_{T44A}$ neurons was significantly larger (figure 1I, WT n=11, $p<0.05$, paired t test; CK1d n=12, $p<0.0001$, paired t test). Moreover, pharmacologically abolishing of tonic inhibition current led to the rescue of hyperpolarized membrane potential in CK1d$_{T44A}$ mutant neurons (figure1J, $p<0.05$, two-way ANOVA, WT n=11, CK1d$_{T44A}$ n=12), suggesting that increased tonic inhibition was indeed the primary cause of hyperpolarized resting V_m in CK1d$_{T44A}$ pyramidal neurons.

No difference in excitatory and inhibitory post-synaptic responses in CK1d$_{T44A}$ L2/3 pyramidal neurons

Neural networks require a precise balance of excitation and inhibition to perform normally. Imbalance between excitatory and inhibitory synaptic transmission may underlay migraine relevant excitability phenotype seen in CK1d$_{T44A}$ animals *in vivo*. To test this hypothesis, we recorded miniature excitatory and inhibitory post-synaptic currents (mE/IPSCs) from S1 L2/3 neurons in presence of 1µM TTX. We found that neither amplitude (p=0.32, Mann Whitney test; WT n=7 and CK1d$_{T44A}$ n=9 neurons; Figure 2C) nor frequency (p=0.97, Mann Whitney test; WT n=7 and CK1d$_{T44A}$ n=9 neurons; Figure 2C) of mEPSCs were significantly different between WT and CK1d$_{T44A}$ neurons. Similarly, when we compared mIPSC amplitude (p=0.33, Mann Whitney test; WT n=9 and CK1d$_{T44A}$ n=15 neurons; Figure 2F) and frequency (p=0.8, Mann Whitney test; WT n=9 and CK1d$_{T44A}$ n=15 neurons; Figure 2F) between WT and CK1d$_{T44A}$ neurons, we did not find a significant difference. These results suggest that AP independent post-synaptic responses to a single quantum of released neurotransmitter, are not significantly different between WT and CK1d$_{T44A}$ neurons.

NMDA receptors are a key component of excitatory synapses as well as a known substrates for CK1 family kinases[26]. Phosphorylation of NMDA receptors through CK1 kinases result in reduced receptor conductance. Hypofunction of kinase activity in CK1d$_{T44A}$ mice[13] could result in reduced phosphorylation, causing increases in NMDA receptor mediated currents[26]. We recorded synaptically evoked AMPA and NMDA mediated currents from L2/3 neurons by stimulating feedforward afferents from L4 and L5$_a$. We found no significant difference in AMPA/NMDA ratio (amplitude or area) in CK1d$_{T44A}$ compared to WT neurons (figure 2G, p=0.24, Mann Whitney test).

Dendritic I_h currents are not altered in L2/3 pyramidal neurons due to CK1d$_{T44A}$ mutation

Somatic voltage responses resulting from post-synaptic currents are shaped and constrained by local dendritic input resistance, which is often determined by the density of hyperpolarization activated (I_h) currents, mediated by cyclic nucleotide gated 'HCN' channels[27]. Reduced I_h currents could not only lead to hyperpolarized dendritic V_m in CK1d$_{T44A}$ neurons, but also result in increased voltage responses to unit synaptic input currents due to reduced dendritic resistance. We isolated I_h currents from L2/3 neurons of both genotype, using the HCN specific antagonist ZD7288. Hyperpolarizing pulses (from -40mV to -100mV, 500ms) were applied to record 'control' currents in presence of pharmacological inhibitor cocktail (see methods). HCN mediated I_h currents were blocked using HCN selective antagonist ZD7288 (25µM) and calculated by subtracting ZD7288 sensitive currents from control currents. We found no difference in the ZD7288 sensitive I_h currents between WT and CK1d$_{T44A}$ neurons (p = 0.95, two-way ANOVA, WT n=8, CK1d$_{T44A}$ n=8; Figure 2H). Combined with the likely low expression of HCN channels reported in L2/3[20], this allowed us to rule out HCN dysfunction as a mechanism of the CK1d$_{T44A}$ phenotype.

Increased action potential frequency in CK1d$_{T44A}$ neurons in response to suprathreshold current injections

Thus far, our data suggested subthreshold hypoexcitability in neurons with no difference in synaptic and dendritic currents. These findings, although seemingly contradictory to our initial hypothesis, only elucidate neuronal activity at rest. Hence, we investigated supratheshold activity in WT and CK1d$_{T44A}$ L2/3 neurons, recording action potential (AP) firing in response to current injection steps. We found no significant difference in the rheobase (figure 3F). However, the V_m thresholds for AP induction were significantly lower in CK1d$_{T44A}$ neurons compared to WT ($p<0.05$, Mann Whitney test, WT n=21, CK1d$_{T44A}$ n=22 Figure 3E). Moreover, CK1d$_{T44A}$ neurons fired action potentials at a higher frequency compared to WT neurons, specifically at higher input current values. This resulted in a significantly higher slope of the AP frequency vs input current curve (F/I slope) in CK1d$_{T44A}$ neurons. (figure 3B, $p<0.05$, two-way ANOVA, Bonferroni's post hoc test, WT n=21 and CK1d$_{T44A}$ n=22; figure 3D, individual neuron comparisons: $p<0.05$, t test, WT n=21 and CK1d$_{T44A}$ n=22). Inter-spike interval between action potentials was also significantly lower in CK1d$_{T44A}$ neurons at the highest input current (400pA) compared to WT (figure 3H, $p<0.05$, two-way ANOVA, WT n=18 and CK1d$_{T44A}$ n=18). This difference was not evident at lower input currents (300pA, figure 3G, p=0.12, two-way ANOVA, WT n=16 and CK1d$_{T44A}$ n=16), suggesting impaired adaptation of action potential firing in CK1d$_{T44A}$ neurons at high intensity input currents. Comparison of AP waveform parameters (figure 3F, AP half-width, p=0.07; figure 3G, AHP duration, p=0.3; figure 3H, AHP amplitude, p=0.14, Mann Whitney test, WT n=21, CK1d$_{T44A}$ n=22)

as well as phase plots of V_m and its first derivative (dV_m/dt, Figure 3J) showed no difference in the depolarization and repolarization phase between $CK1d_{T44A}$and WT neurons. Thus changes in kinetics of APs were not responsible for the reduced inter spike intervals in $CK1d_{T44A}$ neurons.

Tonic inhibitory currents can modulate suprathreshold activity[25]. We found that abolishing tonic inhibitory current with 20µm PTX reduced rheobase in both WT and $CK1d_{T44A}$ neurons (figure 3I, $p<0.05$, paired t test, WT, n=11, $CK1d_{T44A}$, n=12). However, rheobase comparison between PTX treated WT and $CK1d_{T44A}$ neurons was not significantly different (figure 3J, $p<0.05$, two-way ANOVA, WT n=11, $CK1d_{T44A}$n=12). Moreover, the F/I curves of both WT (figure 3K, $p<0.05$, ANCOVA, WT n=11) and $CK1d_{T44A}$ (figure 3L, $p<0.05$, ANCOVA, WT n=12, Figure 3L) neurons were not significantly altered by PTX treatment. Thus, although increased tonic inhibition in $CK1d_{T44A}$ neurons contributed hyperpolarized V_m, it did not affect suprathreshold excitability. Taken together, our dissection of intrinsic and synaptic cellular properties suggested that in spite of hyperpolarized membrane potentials and identical subthreshold membrane and synaptic characteristics, $CK1d_{T44A}$ neurons show a suprathreshold gain of function at higher stimulus intensities.

Frequency dependent adaptation deficit in excitatory synapses of $CK1d_{T44A}$ neurons

To investigate microcircuit dynamics in $CK1d_{T44A}$ mutants, we simulated feedforward L4-L2/3 afferents in acute slices at different frequencies (10, 20, 50Hz) and recorded evoked monosynaptic EPSCs and disynaptic IPSCs. We verified column specificity of stimulation by confirming lack of evoked response from cells outside column (figure 4B and C, $p<0.001$, two-way ANOVA, cells within column and outside column, n=4), to avoid polysynaptic responses. I/O curve of L4-L2/3 synaptic stimulation was not significantly different between WT and $CK1d_{T44A}$ (Figure 4D, p=0.7, ANCOVA, WT n=11, $CK1d_{T44A}$ n=10). WT synapses showed expected adaptation to evoked E/IPSCs as well as paired pulse ratio (PPR), consistent with that described in the literature for adult L4-L2/3 somatosensory cortical synapses[28,29]. Evoked post-synaptic responses reached a steady state with 30 stimuli for EPSCs and 10 stimuli for IPSCs. Following 50 Hz stimulation, the adaptation at $CK1d_{T44A}$ excitatory synapses was significantly impaired, resulting in higher amplitude of evoked steady state currents compared to WT (figure 4F, $p<0.05$, two-way ANOVA, Bonferroni's post hoc test, WT n=11, $CK1d_{T44A}$ n=8). However, at 10 Hz, evoked EPSCs exhibited identical adaptation patterns between WT and $CK1d_{T44A}$ (figure 4H). Response to 20 Hz stimulation showed an intermediate phenotype, with a trend towards blunted adaptation, but no significant difference in steady state currents between WT and $CK1d_{T44A}$ (figure 4G). Interestingly, the increased amplitude of steady state currents was seen exclusively at excitatory synapses, not with evoked inhibitory currents (figure 4I to K, $p>0.05$, two-way ANOVA, Bonferroni's post hoc test, WT n=11, $CK1d_{T44A}$ n=8). Moreover, across all stimulation frequencies, evoked E/IPSCs revealed no significant difference in the PPR between WT and $CK1d_{T44A}$ (figures 4F to K insets, $p>0.05$, Mann Whitney test, WT n=11, $CK1d_{T44A}$ n=8). These results suggest high frequency dependent adaptation failure at $CK1d_{T44A}$ excitatory synapses.

Enhanced RRP replenishment underlies impaired adaptation at $CK1d_{T44A}$ excitatory synapses

The rapid adaptation to repeated stimuli is a presynaptic phenomenon, due to relative depletion and replenishment of the readily releasable pool (RRP), a process that has biphasic kinetics[23,24,30]. When subjected to sustained stimulation, the RRP initially depletes quickly as the rate of release is greater than the rate of replenishment. Later, RRP replenishment maintains equilibrium with RRP release, as post-synaptic responses reach a steady state[23,24]. Kinetics of RRP replenishment can be resolved using cumulative amplitude plots of post-synaptic responses. We dissected biphasic kinetics of RRP replenishment with the single phase exponential fitted to the initial rise (fast RRP) and linear regression fitted through the steady state (slow RRP) with Y intercept of the linear regression is an indicator of the size of the RRP (figure 5A)[24,30]. The linear regression slopes of cumulative E/IPSC amplitude plots were not significantly different between WT and CK1d$_{T44A}$ at any stimulation frequency (figures 5B to G, top, $p>0.05$, ANCOVA, WT n=11, CK1d$_{T44A}$ n=8). Similarly, the Y intercept values of the linear regression were not different at any frequency for EPSC or IPSC plots between WT and CK1d$_{T44A}$ (figure 5B-G bottom right). Therefore, WT and CK1d$_{T44A}$ had similar slow RRP replenishment rate and RRP size. However, the single exponential rise of EPSC cumulative amplitude plots was significantly faster in CK1d$_{T44A}$ at both 50 Hz and 20 Hz (figure 5B and C top, $p<0.0001$, F test with AIC correction, WT n=11, CK1d$_{T44A}$n=8), along with significantly higher time constant (τ) values in CK1d$_{T44A}$ (figure 5B and C bottom left, $p<0.05$, Mann Whitney test, WT n=11, CK1d$_{T44A}$n=8). No difference in the initial exponential rise was seen in the cumulative EPSCs at 10Hz as well as cumulative IPSCs at every stimulation frequency (figures 5E to G). This suggests that the frequency dependent adaptation failure at CK1d$_{T44A}$ excitatory synapses is due to more efficient 'fast' replenishment of the RRP.

Impaired adaptation at excitatory synapses leads to a net excitatory shift in excitation-inhibition balance

In a separate set of experiments to isolate fast RRP replenishment in evoked EPSCs, we stimulated the L4-L2/3 synapse with only 10 stimuli not allowing the post-synaptic responses to reach steady state. Similar to our experiments with 30 stimuli, we found that the evoked EPSCs failed to adapt at CK1d$_{T44A}$ synapses, specifically at 50Hz (figure 6C, $p<0.05$, two-way ANOVA, WT n=8, CK1d$_{T44A}$ n=13). However, there was no difference in the PPR between genotypes (figure 6C, inset). We also found that single phase exponentials fitted to the cumulative amplitude plots were significantly different between WT and CK1d$_{T44A}$ at all stimulation frequencies ($p<0.05$, Two-way ANOVA, WT n=8, CK1d$_{T44A}$ n=13 Figure 6F to H), with significantly higher time constant (τ) values in CK1d$_{T44A}$ (figure 6F inset $p<0.05$, Mann Whitney test, WT n=8, CK1d$_{T44A}$n=13). These results recapitulate our previous observation of enhanced fast RRP replenishment at CK1d$_{T44A}$ excitatory synapses.

We then wanted to investigate whether high frequency stimulation perturbs excitation/inhibition (E/I) balance in CK1d$_{T44A}$ microcircuits. We used amplitudes of evoked E/IPSCs to 10 stimuli from the same neurons to generate E/I ratios and compared them across genotype. We found a significant excitatory shift in CK1d$_{T44A}$ compared to WT synapses at both 50 and 20 Hz stimulation (figure 6I, 50Hz: $p<0.0001$, Figure 6J, 20Hz: $p<0.05$, two-way ANOVA, WT n=8, CK1d$_{T44A}$n=13) but not 10 HZ stimulation (figure 6K). Thus, frequency dependent impairment of adaptation at CK1d$_{T44A}$ excitatory synapses result in a net excitatory shift in L4-L2/3 synapses.

Adaptation deficit at CK1d$_{T44A}$ excitatory synapses is independent of presynaptic NMDAR function

Recent evidence suggests that RRP replenishment may be modulated by presynaptic NMDA receptors at cortical synapses[31]. CK1 isoforms phosphorylate NMDA receptors, especially NR2B subunits found presynaptically in adult cortex, decreasing their conductance[26]. We hypothesized that the reduced kinase activity in CK1d$_{T44A}$ mice[13] could lead to an increase in presynaptic NMDA currents, resulting in a gain of presynaptic function consistent with the observed phenotype. To test this hypothesis we eliminated the possible role of post-synaptic NMDARs with intracellular application of MK801 (10µM) via patch pipette, and isolated presynaptic NMDA currents by applying AP5 (50µM) to the bath (figure 7A). Intracellular MK801 that blocked post-synaptic NMDA currents did not alter excitatory synaptic adaptation in WT or CK1d$_{T44A}$ neurons (Supplimentary figure). More importantly, bath application of AP5 had no effect on the increased steady state currents in CK1d$_{T44A}$ neurons (figure 7C right, $p>0.05$, two-way ANOVA, CK1d$_{T44A}$ MK801 and CK1d$_{T44A}$ MK801+AP5 n=7). Therefore, pre-synaptic NMDARs do not likely contribute to the elevated excitatory steady state currents seen at CK1d$_{T44A}$ synapses. Moreover, kinetic analysis of cumulative amplitudes revealed that bath application of AP5 did not affect either linear regression slopes (figure 7C right, $p>0.05$, ANCOVA, CK1d$_{T44A\ MK801}$ and CK1d$_{T44A}$ MK801+AP5 n=7) or the single phase exponential rise (figure 7C right, $p>0.05$, F test with AIC correction, CK1d$_{T44A}$ MK801 and CK1d$_{T44A}$ MK801+AP5 n=7) that quantify components of RRP. This suggests that the adaptation deficit due to enhanced fast RRP replenishment in CK1d$_{T44A}$ synapses was independent of pre-synaptic NMDAR function.

Inhibition of recurrent excitation abolished increase in action potential frequency in CK1d$_{T44A}$ neurons

CK1d$_{T44A}$ neurons showed larger number of APs with increased current intensities (180-200pA suprathreshold current), compared to WT. At such high intensities, neurons typically fire APs at 30-40 Hz[32]. Due to impairment of excitatory synaptic adaptation at higher frequencies, recurrent excitation (feedback excitation generated due to neuronal activity) on CK1d$_{T44A}$ neurons can be amplified[33]. To test whether increased recurrent excitation is responsible for increased AP firing, we recorded F/I curves in presence of glutamate receptor antagonists. Post-synaptic NMDARs were blocked using 10µM MK801 in the patch pipette and AMPARs with 20µM CNQX applied in the bath. Interestingly, abolishing recurrent excitation with post-synaptic glutamate receptor antagonists normalized input current dependent increase in AP frequency seen in CK1d$_{T44A}$ neurons (figure 7H left: $p>0.05$, two-way ANOVA, WT n=7, CK1d$_{T44A}$ n=10). It also rescued differences in F/I curve slopes between genotypes (figure 7H right: $p>0.05$, two-way ANOVA, WT n=7, CK1d$_{T44A}$ n=10), implying that increased AP firing in CK1d$_{T44A}$ neurons at higher current intensities was due to amplified recurrent excitation.

Excitable sensory cortical circuits in CK1d$_{T44A}$ mice *in vivo*

We wanted to test whether the cellular and synaptic phenotypes we observed *in vitro,* were reflected in sensory network phenotypes *in vivo*. Cortical slow oscillations (1Hz), expressed as depolarized ‘up state’ and hyperpolarized ‘down states’, represent a form of dynamic gain modulation[34,35]. The depolarized ‘up states’ increase the likelihood of neuronal AP generation

upon feedforward stimulus[35–37]. We recorded membrane responses of S1 L2/3 pyramidal neurons to network driven up and down states using *in vivo* current clamp recordings. Consistent with our *in vitro* findings, neuronal resting V_m were significantly hyperpolarized in CK1d$_{T44A}$ mice *in vivo* ($p<0.05$, Mann Whitney test, WT N=5 and CK1d$_{T44A}$ N=5, figure 8B) suggesting that *in vitro* cellular phenotypes were similarly operant *in vivo.* Comparison of 'up states' revealed that their duration was significantly increased in CK1d$_{T44A}$ mice compared to WT (figure 8C, $p < 0.001$; 2-sample KS test; WT N=5 and CK1d$_{T44A}$N=5). The percent time neurons spent in 'up states' was also significantly higher in CK1d$_{T44A}$ mice (figure 8D, $p<0.05$, Mann Whitney test, WT N=5 and CK1d$_{T44A}$N=5,). V_m variance during up states was also significantly greater in CK1d$_{T44A}$ compared to WT neurons ($p<0.0001$, Mann Whitney test, WT N=5 and CK1d$_{T44A}$ N=5). The 'up state' phenotype in CK1d$_{T44A}$ mice is consistent with increase in local network excitability, as the phenotype is shared by mouse models of other neurological disorders like epilepsy[36].

Neurons exhibit excitatory (V_{clamp} -70mV) and inhibitory (V_{clamp} 20mV) synaptic currents during up states, which can be quantified as E/I ratio. We found a robust increase in the half width as well as area of excitatory (figure 8F, $p<0.05$, 2-sample KS test, WT N=5 and CK1d$_{T44A}$ N=5) compared to inhibitory (figure 8I $p>0.05$, 2-sample KS test) current recorded during up states in CK1d$_{T44A}$ mice, resulting in a significant shift in E/I balance towards excitation in CK1d$_{T44A}$ mice (figure 8I, $p<0.05$, 2-sample KS test, WT N=5 and CK1d$_{T44A}$ N=5). This results, taken together with 'up states', provides a robust evidence of excitable sensory networks in CK1d$_{T44A}$ mice.

Discussion

Migraine is a common neurological disorder that severely impairs quality of life and imposes a serious economic burden on society[1,3]. Apart from the headaches and craniofacial pain, a key feature in migraine is sensory network excitability[4]. One third of migraine attacks are preceded by sensory hallucinations called 'auras', triggered by a self-propagating cortical wave of neuro-glial depolarization called cortical spreading depression (CSD)[4,7]. CSD is followed by long term perturbation of subcortical sensory activity, of cortical synaptic transmission[18] and sensory processing[38], which may contribute to a global increase in pan-multi-sensory gain (photophobia, phonophobia, allodynia etc.)[5,6]. Similar multisensory gain phenotypes occur in migraine without aura; thus other mechanisms likely converge to activate the overall network response. Interestingly, migraineurs report reduced habituation to repeated sensory stimuli under normal conditions, which may contribute to sensory hypersensitivity[8,9]. However, the precise molecular and cellular mechanisms that render migraineurs susceptible to such excitability are poorly understood.

$CK1d_{T44A}$ mutant mice: a new model of non-hemiplegic migraine with obscure mechanisms

Although migraine is more commonly polygenic[4], animal models of monogenic forms of the disorder offer a unique opportunity for mechanistic dissection. Thus far, mouse models of migraine have carried mutations identified from patients with a severe monogenic form, familial hemiplegic migraine (FHM 1 and 2)[12]. Both these models share common a migraine phenotype (increased susceptibility to CSD evoked in sensory cortex)[11], as well as a common mechanism (gain of function at glutamatergic synapses either by increased glutamate release in FHM1[39,40] or impaired glutamate reuptake in FHM2[41]). Apart from reduced CSD threshold, excitable sensory network features are a common theme in migraineurs and migraine models alike[4]. Familial hemiplegic migraine models show increased output at excitatory synapses[39,41] and enhanced hippocampal long term potentiation[42].

More recently, a loss of function mutation in the casein kinase-1 delta gene ($CK1d_{T44A}$) was identified from two families with a combination of familial migraine with aura and advanced sleep phase syndrome[13,43]. Mice harboring this mutation show migraine relevant phenotypes including increased CSD susceptibility and increased sensitivity to the migraine trigger[13]. However, the CK1d protein is ubiquitously expressed in multiple cell types across various brain regions and developmental stages and interacts with different downstream signaling molecules[14]. Thus, though the molecular moiety responsible is identified, the circuit mechanisms by which this molecule acts are not immediately obvious. Understanding these mechanisms are is important, as it they may offer insights into novel therapeutic targets for phenotypically normal migraine.

Impaired adaptation at excitatory synapses contributes to hyperexcitability within sensory networks

In this study, we used *in vitro* whole cell slice electrophysiology as our primary technique to dissect cellular and synaptic mechanisms. We found that $CK1d_{T44A}$ pyramidal neurons had hyperpolarized resting V_m due to increased tonic inhibitory current. However, we observed increased amplitude of the steady state evoked excitatory currents in $CK1d_{T44A}$, due to impaired

adaptation at high stimulation frequencies. Similarly, CK1d$_{T44A}$ neurons fired APs at significantly higher frequencies with increased intensities of suprathreshold current injections. Increased frequency of AP was abolished by subjecting CK1d$_{T44A}$ neurons to glutamate receptor antagonists (AMPA and NMDA), suggesting the role of recurrent synaptic excitation induced by higher intensity of injected current. These results show that although CK1d$_{T44A}$ neurons are apparently hypoexcitable at resting state, the network becomes hyperexcitable when presented with intense stimuli. Finally, *in vivo* whole cell recordings from CK1d$_{T44A}$ animals revealed increased duration and V_m variance at cortical 'up states'. These experiments show that the cellular and synaptic mechanisms we observed *in vitro* are likely operant in excitatory local networks *in vivo*.

Increased sensory gain is a key feature in migraine, with migraineurs reporting lack of habituation to repeated sensory stimuli[8,9,44]. Although synaptic adaptation is regarded as a prominent mechanism for sensory gain modulation and habituation[45,46], it remains poorly investigated in migraine models. Excitatory synapses rapidly adapt to repeated sensory stimuli compared to slow adaptation at inhibitory synapses[47]. Fast adaptation at excitatory synapses moderates the intensity of feedforward sensory signaling that is necessary for perception without overactivating the circuit[48,49]. The results in this study are consistent with our previous findings showing blunted adaptation to repeated sensory stimuli *in vivo* following a migraine relevant perturbation (CSD) in WT mice[38]. Adaptation failure is thus present in two different migraine models, (a genetic model and a model of migraine aura), potentially providing a circuit mechanism for the habituation failure to repeated stimuli reported in migraineurs[9].

Improved RRP turnover - a possible mechanism for the CK1d$_{T44A}$ synaptic adaptation phenotype

Our *in vitro* findings showing adaptation impairment at excitatory synapses strongly implicate presynaptic mechanisms[50,51]. The amplitudes of evoked currents at steady state depends on the size and replenishment rate of readily releasable pool (RRP), which is a small fraction of vesicles ready for immediate release in densely packed presynaptic boutons[24]. Upon stimulation, these vesicles are readily released, depleting the RRP. The probability of vesicular release within the RRP determines synaptic strength. Replenishment of the RRP determines release in response to consecutive stimuli, regulating short-term synaptic adaptation to multiple stimuli[52]. The RRP is never completely depleted following repeated stimulations, as it is replenished from a distinct pool of vesicles known as the reserve pool[23], through a delicate balance between vesicular endo- and exocytosis[53]. Although disparate at first, the rates of depletion and replenishment of the RRP reach equilibrium eventually, resulting in steady state post-synaptic responses. This generates two distinct rates of RRP replenishment- RRP is depleted rapidly at first (fast) and then replenishment is at equilibrium with release (slow)[23,54]. We found that the fast component of RRP replenishment was more efficient in CK1d$_{T44A}$ neurons, with the slow component at steady state not different from WT. Interestingly, our finding of enhanced RRP replenishment in CK1d$_{T44A}$ model is phenotypically consistent with studies in the FHM1 model[55] – another circuit phenotype that is convergent across very different migraine models.

Presynaptic NMDA receptors have been shown to specifically mediate evoked release[31] and are implicated in regulating vesicle replenishment at different cortical synapses, either through

Ca^{+2}/calmodulin dependent or several other downstream molecular mechanisms[31,56–58]. NMDA receptors are a known substrate for CK1 family of kinases, most prominently affecting NR2B subunit containing receptors[26]. Presynaptic NMDARs are implicated regulation of in presynaptic plasticity, functioning as coincidence detectors for high frequency activity[59,60]. In adult cortex, NR2B containing NMDA receptors are mostly found at presynaptic terminals[61,62]. Phosphorylation of NMDA receptors by CK1 kinases leads to reduced NMDA currents. We hypothesized that loss of function mutation in $CK1d_{T44A}$ would lead to increase in presynaptic NMDA currents resulting in gain of presynaptic function. However, pharmacological interventions used to selectively block pre-synaptic NMDA receptors[63,64] revealed no significant effect on the amplitude excitatory steady state currents, suggesting a presynaptic NMDA-independent mechanism.

The RRP is thought to consist of either all of the docked vesicles or a subset of them, with some studies suggesting that some undocked vesicles also contribute to the RRP through rapid recruitment[24]. The vesicles become part of the RRP though a molecular process called 'vesicle priming'. *In vitro* fusion assays using knockout animals show that presynaptic proteins like RIM, Munc13, and Munc18 are essential for vesicle priming[65]. Current models suggest RIM interacts with Munc13 to activate release cites, while Munc13 and Munc18 mediate assembly of SNARE complex[65,66], making them critical for vesicle docking and fusion. Although interactions between $CK1d_{T44A}$ and these presynaptic proteins are unknown, improved vesicle docking is a plausible mechanism. Another potential mechanism for the presynaptic gain of function involves synaptic vesicle proteins. CK1 kinases not only co-localize with synaptic vesicular markers[67], but are shown to phosphorylate a specific subset of vesicle specific proteins, namely SV2. Phosphorylation of $SV2_A$ protein at Thr84 by CK1 family kinases controls the retrieval of synaptotagmin-1, a calcium sensor for the SNARE complex mediating release of synaptic vesicles[68,69]. CK1d was also found to specifically interact with the SNARE associated protein snapin, which was originally identified as a SNAP25 interacting protein that regulates the association of the calcium sensor synaptotagmin-1 with the SNARE complex[15]. More recent evidence suggests that snapin also interacts with a non-neuronal yet homologous SNAP23 protein, which facilitates vesicle transport[70]. These data support a role of CK1d in the regulation of synaptic vesicle release/transport processes, but which specific protein/protein interaction is involved requires further investigation.

'Up state' phenotype in $CK1d_{T44A}$ animals indicates hyperexcitable sensory networks *in vivo*

Sensory perception is a mutlinetwork process and the mechanisms for altered perception span well beyond the single synapse level[71]. Migraine as a disorder of sensory gain is unlikely to be understood without understanding network-wide mechanisms. Cortical slow oscillations are a well-characterized form of dynamic gain modulation[72]. Our *in vivo* investigations of cortical slow oscillations show increased up state duration and membrane voltage variance, in spite of hyperpolarized resting membrane potentials. Slow oscillations (up and down states) occur in sleep and are typically measured under urethane anesthesia, but they also occur during quiet wakefulness[72,73]. Depolarized cortical up states provide a window for AP generation, by increasing the probability of membrane potential reaching AP threshold. Hence, an up state can act as a coincidence detector for feedforward signal transduction[73,74]. We found that sensory neurons from

CK1d$_{T44A}$ animals exhibit increased duration as well as V_m variance during 'up states', therefore increasing the probability of action potential firing upon receiving feedforward sensory signal [37,75]. Increased 'up state' frequency and duration are often regarded as markers for network excitability - e.g. in epilepsy[35,36]. Like epilepsy patients, migraine patients show alterations in both high- and low-frequency cortical and thalamocortical oscillations; the latter are likely correlates of up-states[44,76]. We also found that CK1d$_{T44A}$ neurons receive significantly longer excitatory post-synaptic currents during upstates, tipping the excitatory-inhibitory balance towards net excitation. This is consistent with our *in vitro* findings that indicate an increase in excitatory-inhibitory ratio of currents evoked at higher stimulation frequency. The convergent *in vitro* and *in vivo* findings provide insight on the mechanisms of sensory gain at the network level that may be relevant beyond the CK1d$_{T44A}$ mutation. Analogous to the common phenotype of CSD, there are multiple ways to arrive at the common circuit phenotype.

Increased tonic inhibitory current in CK1d$_{T44A}$ neurons: compensatory mechanism or consequence of network excitability?

Our *in vitro* dissection shows that CK1d$_{T44A}$ neurons experience a significantly higher tonic inhibitory current, which is responsible for their hyperpolarized resting V_m. Pharmacological blockade of inhibitory currents reveled that increased tonic inhibition was responsible for hyperpolarized membrane potentials; however it did not have a significant effect on suprathreshold cellular properties in CK1d$_{T44A}$ neuro ns compared with WT. Tonic inhibitory currents are mediated by δ subunit containing extra-synaptic $GABA_A$ receptors[25]. An increase in tonic inhibition can be attributed to a gain in number or function of extra-synaptic $GABA_A$ receptors. Likewise, presynaptic mechanisms can also lead to increase tonic inhibitory currents[77,78]. The magnitude of tonic inhibitory current is dependent on the balance between GABA release and reuptake, and thus varies with the intensity of local network activity[78,79]. GABA transporters, responsible for GABA reuptake, are near equilibrium under baseline conditions[80], thus only moderate cell depolarization with brief bursts of action potentials should be sufficient for GABA transporter reversal[81,82], resulting in non-vesicular release of GABA. Moreover, asynchronous GABA release during prolonged high frequency stimulation was shown to be a major contributor of tonic inhibition[83]. Hence, increased tonic GABA current may actually be a result of network hyperexcitability found in CK1d$_{T44A}$ animals, due to a presynaptic gain of function.

Gain of function at glutamatergic synapses as a unifying mechanism linking multiple monogenic migraine models

CK1d$_{T44A}$ along with models of hemiplegic migraine (FHM1 and 2) show an increased susceptibility to CSD, consistent with increased sensory circuit excitability. The mechanism underlying this increased excitability is well established in FHM1 and 2, because the proteins involved have roles that are immediately attributable. FHM1 is a gain of function mutation of a P/Q type Ca^{+2} channel subunit (CaV2.1) that results in larger presynaptic calcium currents[12,40], and increased synaptic release at excitatory glutamatergic synapses[39]. FHM2 is a loss function mutation of an Na^+/K^+ ATPase subunit that is essential to astrocytic glutamate transporter function, and results in impaired glutamate and K^+ reuptake at the excitatory synapse[12,41]. We found that the CK1d$_{T44A}$ mutation also excibited a gain of function the glutamatergic synapse, in

564 the form of high frequency dependent impairment of presynaptic adaptation. Although the precise
565 protein/protein interaction remains unexplored, these results provide a unifying synaptic
566 mechanism for migraine relevant phenotypes across different models. Interestingly, this
567 glutamatergic gain of function is larger in FHM 1 and 2 than in $CK1d_{T44A}$, potentially consistent
568 with the differences in severity between hemiplegic and non-hemiplegic forms of migraine[84]. The
569 cellular and synaptic gain of function found in $CK1d_{T44A}$ in response to higher stimulus intensity
570 recapitulates the intensity dependent hypersensitivity phenotype found in most migraineurs. The
571 findings in this study not only establish $CK1d_{T44A}$ as an effective model for non-hemiplegic forms
572 of migraine, but also provide key mechanistic insights to understand migraine as a disorder of
573 network excitability more broadly.

574

575

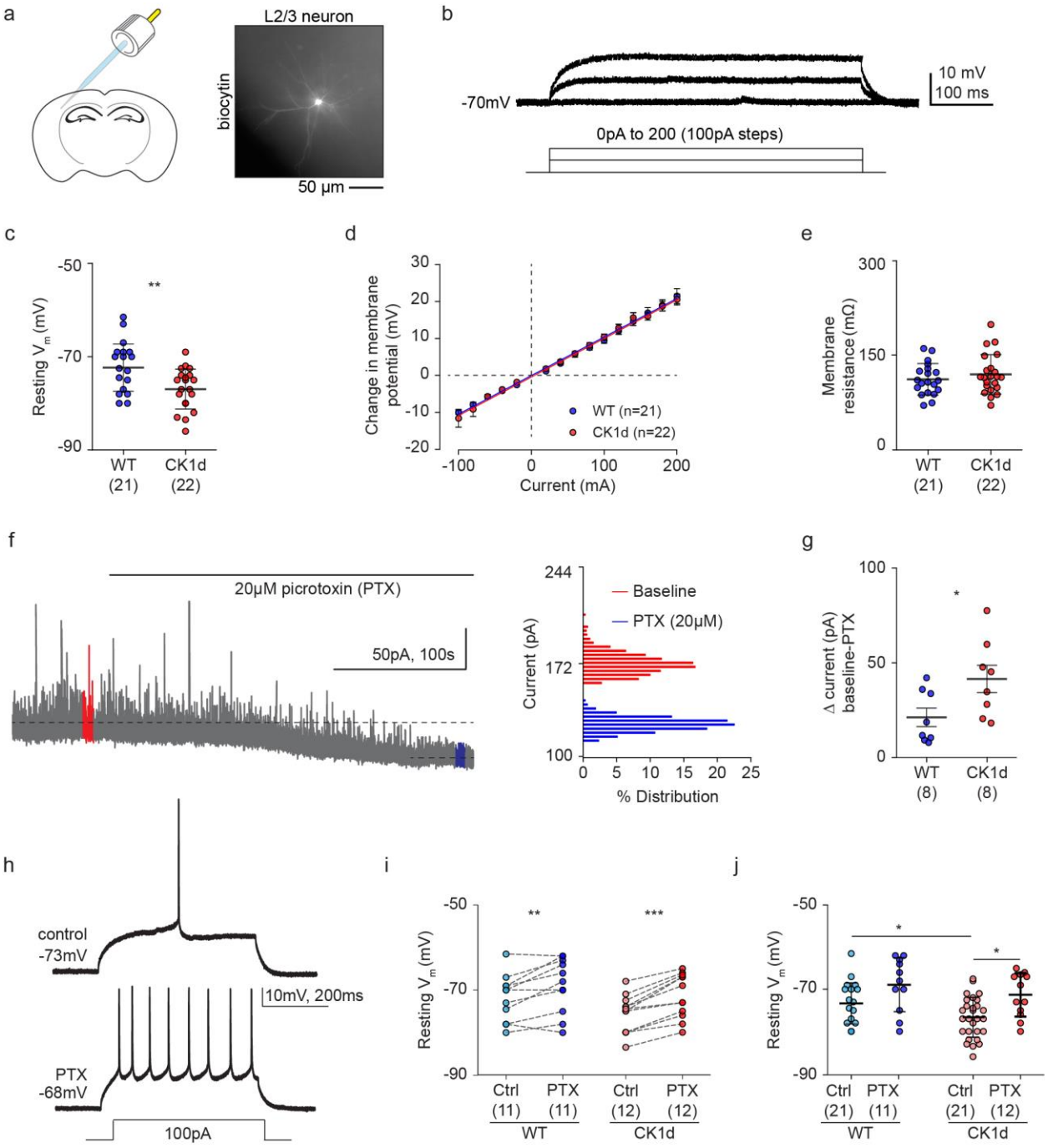

Figure 1: Hyperpolarized membrane potentials due to increased tonic inhibition in CK1d$_{T44A}$ neurons

a] Schematic showing *in vitro* whole cell patch clamp set up using acute coronal sections of mouse brain (top) and a representative image of a typical excitatory L2/3 neuron labelled with biocytin during patch clamp experiment. b] Representative traces showing membrane voltage responses to subthreshold current injections (from 0pA to 200 at 100pA steps) recorded in I_{clamp} mode. c] Comparison of resting membrane potentials (Vm) between WT and CK1d$_{T44A}$ neurons revealed that CK1d$_{T44A}$ neurons were significantly hyperpolarized ($p<0.05$, t test, WT n=21, CK1d$_{T44A}$ n=22). d] Comparison between slopes of the IV curves of WT and CK1d$_{T44A}$ neurons (Linear regression fitted through IV curves, WT slope =0.104, CK1d$_{T44A}$ slope =0.103, p= 0.99, analysis of covariance (ANCOVA)). e] Comparison of input resistance values for individual neurons between WT and CK1d$_{T44A}$ ($p=0.36$, t test, WT n=21, CK1d$_{T44A}$ n=22). f] Left: Representative trace showing reduction in tonic inhibitory holding current recorded at Vclamp 10mV, after application of 20µM picrotoxin ($GABA_a$ antagonist). Tonic inhibitory currents or picrotoxin sensitive currents are calculated by subtracting currents recorded after picrotoxin treatment from baseline (control) current. Right: % Distribution histogram shows narrow distribution with reduced mean currents after picrotoxin application (blue) compared to baseline (red). g] Tonic inhibitory currents (ΔpA) were significantly higher in CK1d$_{T44A}$ neurons compared to WT ($p<0.05$, Mann Whitney, WT n=8, CK1d$_{T44A}$ n=8). h] Representative traces showing resting membrane potential as well as voltage response to depolarizing current pulse before and after picrotoxin application. i] Difference in the resting membrane potential between individual WT neurons ($p<0.05$, paired T test, n=11) as well as F] CK1d$_{T44A}$neurons ($p<0.05$, paired T test, n=12) before and after picrotoxin treatment. j] Pharmacological blockade of tonic inhibitory current lead to rescue of hyperpolarized membrane potentials in CK1d$_{T44A}$neurons ($p<0.05$, WT ctrl n=21 vs CK1d$_{T44A}$ctrl n=21, $p<0.05$ CK1d$_{T44A}$ctrl vs CK1d$_{T44A}$ptx, p=0.39 WT ptx n=11 vs CK1d$_{T44A}$ptx n=12, Two-way ANOVA).

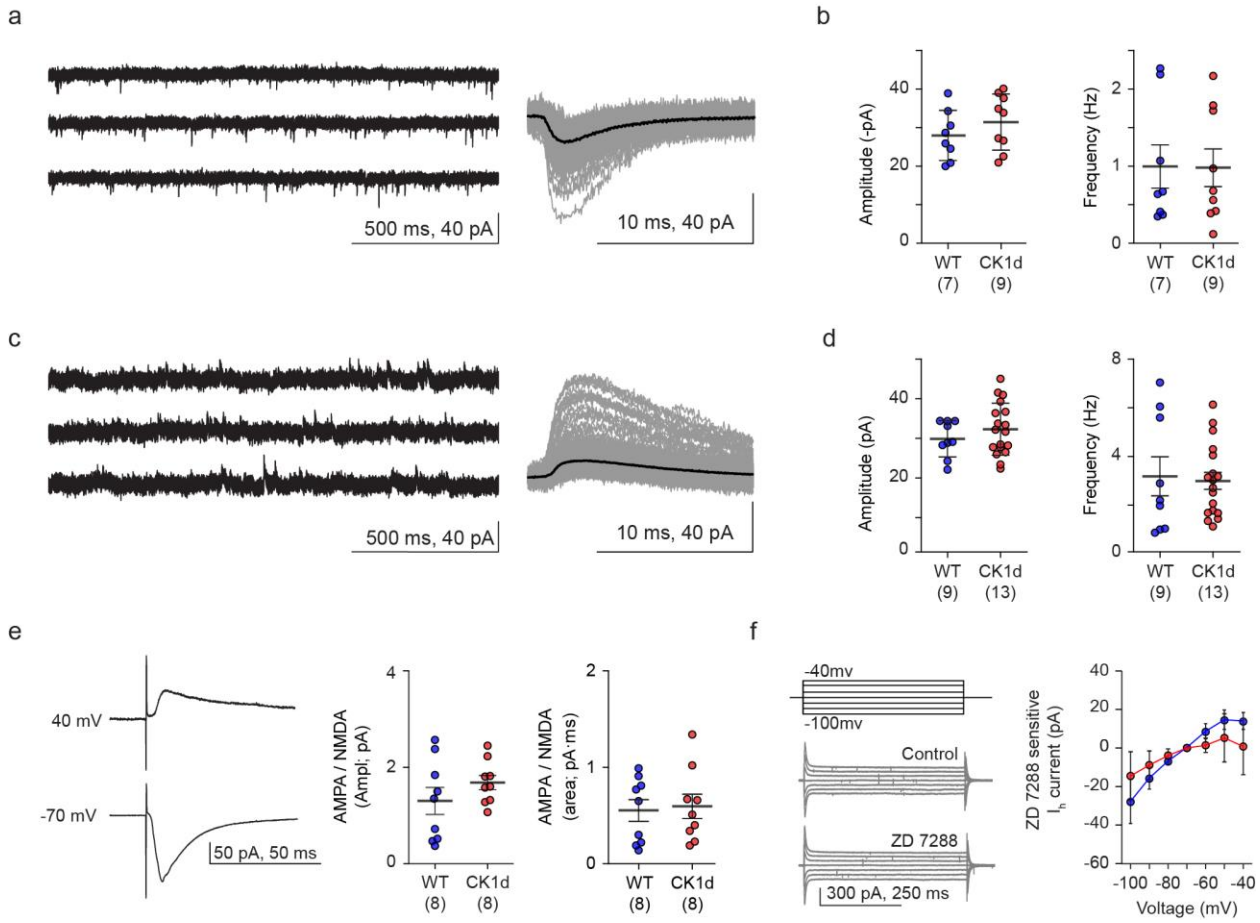

607

Figure 2: No difference in the synaptic and dendritic currents between WT and CK1d$_{T44A}$ neurons

a] Representative traces of miniature excitatory post synaptic currents (mEPSC) recorded by clamping neurons at -70mV in the presence of 1µM tetrodotoxin (TTX). Inset: traces of individual mEPSC events (gray) and average value for all events (black) for a single neuron. b] No significant difference was found in mEPSC amplitude (left, p=0.32, t test, WT n=7, CK1d$_{T44A}$ n=9) as well as mEPSC frequency (right, p=0.97, t test, WT n=7, CK1d$_{T44A}$ n=9) between WT and CK1d$_{T44A}$ neurons. c] Representative traces of miniature inhibitory post synaptic currents (mIPSC) recorded by clamping neurons at 10mV in the presence of 1µM tetrodotoxin (TTX). Inset: traces of individual mIPSC events (gray) and average value for all events (black) for a single neuron. d] No significant difference was found in mIPSC amplitude (left, p=0.33, t test, WT n=9, CK1d$_{T44A}$ n=15) as well as mIPSC frequency (right, p=0.8, t test, WT n=9, CK1d$_{T44A}$ n=15) between WT and CK1d$_{T44A}$ neurons. e] Left: Representative traces of evoked AMPA currents (bottom, V_{clamp} -70mV) and evoked NMDA currents (top, V_{clamp} 40mV) recorded from L2/3 excitatory neurons upon stimulation of L4/L5$_a$ afferents. Right: no difference was found either in AMPA/NMDA ratio of amplitude (p=0.24, t test, WT n=8, CK1d$_{T44A}$ n=8) or area (p=0.76, t test, WT n=8, CK1d$_{T44A}$ n=8) between WT and CK1d$_{T44A}$ neurons. f] Left: Representative traces of currents recoded in V_{clamp} mode in response to hyperpolarizing voltage steps (from -40 to -100mV). All currents were recorded in the presence of cocktail of inhibitors (1µM TTX, 10 µM PTX, 10 µM CNQX, 10 µM XE991, 3mM TEA) to block all voltage as well as ligand gated currents. HCN channel mediated I_h currents were isolated using specific antagonist ZD7288 (25µM). Right: comparison of I_h currents or normalized ZD7288 sensitive currents between WT and CK1d$_{T44A}$ neurons at voltages ranging from -40 to -100 mV revealed no significant difference between the two groups (p>0.05, two-way ANOVA, Bonferroni's post hoc test revealed non-significant differences at individual voltage steps, WT n=8, CK1d$_{T44A}$ n=8).

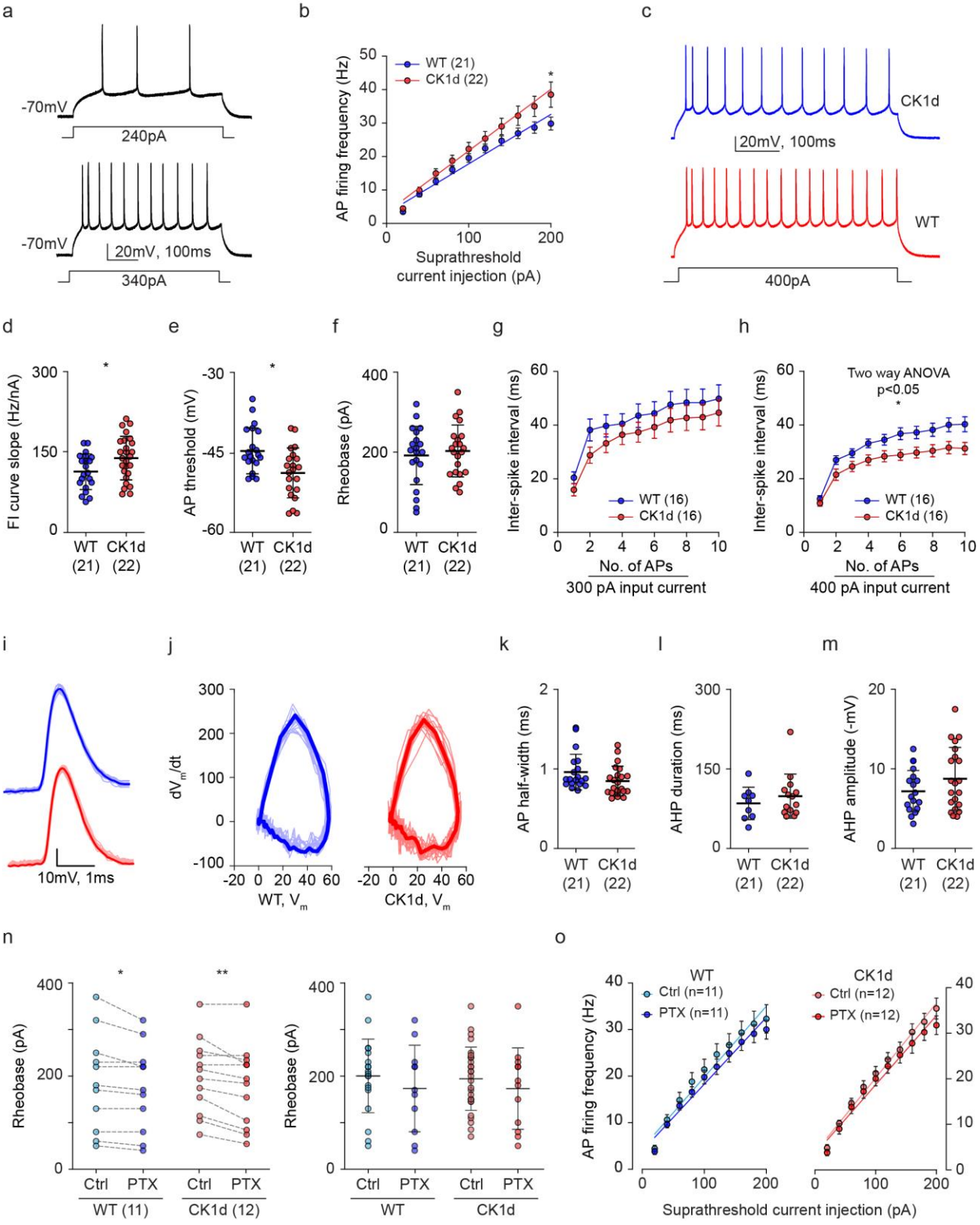

Figure 3: Increased frequency of action potentials in CK1d$_{T44A}$ neurons at higher suprathreshold input currents

a] Representative traces of L2/3 excitatory neurons firing action potentials to suprathreshold current injections. b] Comparison of action potential firing frequencies at different input current values (F/I curves) between WT and CK1d$_{T44A}$ neurons. F/I curves were significantly different between WT and CK1d$_{T44A}$ mice, especially at higher input currents. ($p<0.0001$, two-way ANOVA, at 200pA, $p<0.05$, Bonferroni's post hoc test). Slopes of F/I curves were also found to be significantly different between WT and CK1d$_{T44A}$ neurons (Linear regression fitted through F/I curves, WT slope =0 0.148, CK1d$_{T44A}$ slope = 0.184, $p= 0.012$, analysis of covariance (ANCOVA)). c] Representative traces of WT (top, blue) and CK1d$_{T44A}$ (bottom, red) neurons firing action potentials in response to 400pA current injection. d] Comparison of F/I curve slopes calculated for individual neurons between WT and CK1d$_{T44A}$neurons revealed that CK1d$_{T44A}$ had significantly higher F/I slopes ($p<0.05$, Mann Whitney test, WT n=21, CK1d$_{T44A}$ n=22). e] The membrane voltage thresholds values at which individual neurons started firing action potentials were significantly lower in CK1d$_{T44A}$ neurons ($p<0.05$, non-parametric T test, WT n=21, CK1d$_{T44A}$ n=22). f] No significant difference in rheobase between WT and CK1d$_{T44A}$ neurons ($p=0.59$, t test, WT n=21, CK1d$_{T44A}$ n=22). g] Comparison of inter spike interval (ISI) between WT and CK1d$_{T44A}$ neurons was not significantly difference at 300pA ($p<0.0001$, two-way ANOVA, WT n=16, CK1d$_{T44A}$ n=18). h] However the difference in ISI was statistically significant at 400pA ($p < 0.0001$, two-way ANOVA, WT n=16, CK1d$_{T44A}$ n=18). i] Representative AP traces (blue: WT, red: CK1d$_{T44A,}$ dark traces indicate averages) as well as j] phase plots V_m differentials (dV_m/dt vs V_m) showing no difference in the AP waveforms between WT and CK1d$_{T44A}$ neurons. No difference was observed in k] AP half-width ($p=0.45$, t test, WT n=21, CK1d$_{T44A}$ n=22), l] After-hyperpolarization or AHP duration ($p=0.97$, t test, WT n=21, CK1d$_{T44A}$ n=22) as well as m] AHP amplitude ($p=0.82$, t test, WT n=21, CK1d$_{T44A}$ n=22). n] Although picrotoxin reduced rheobase in neurons across the two genotypes (left: $p<0.05$, paired t test, WT n=11, CK1d$_{T44A}$ n=12), comparison between picrotoxin treated CK1d$_{T44A}$ and WT neurons showed no difference (right: $p>0.05$, two-way ANOVA). o] Picrotoxin did not FI slopes in both WT ($p<0.05$, ANCOVA, n=11) as well as CK1d$_{T44A}$ ($p<0.05$, ANCOVA, n=12).

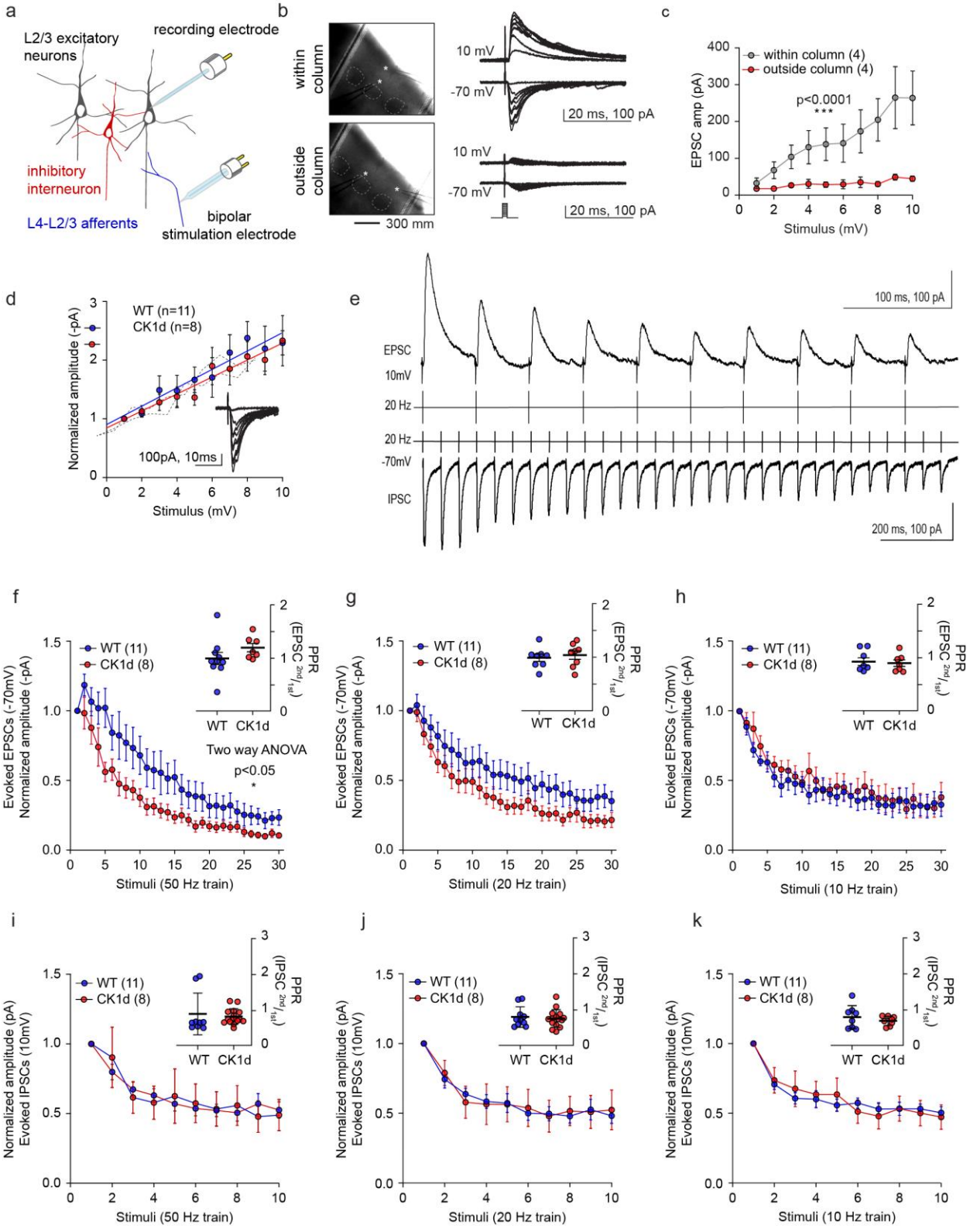

667

Figure 4: Frequency dependent adaptation deficits due to higher steady state current at CK1d$_{T44A}$ excitatory synapse

a] Schematic representation of L2/3 cortical microcircuit showing placement of stimulation as well as recording electrodes. b] Images and representative traces and showing experimentally evoked EPSC and IPSC responses recorded from neurons within (top) and outside (bottom) of cortical column c] Quantification of EPSC amplitudes to increasing stimulus intensities for within column and outside column stimulation ($p<0.0001$, two-way ANOVA, within column n=4, outside column n=4). d] Input-output relationship between WT and CK1d$_{T44A}$ to selected microsimulation intensities was not significantly different ($p=0.7$, ANCOVA, WT n=11, CK1d$_{T44A}$ n=8). e] Representative traces showing evoked EPSC and IPSC responses to trains of 30 and 10 stimuli respectively, at 20Hz. f] Normalized EPSC Steady state evoked EPSC response to 50Hz stimulus train were significantly higher at CK1d$_{T44A}$synapse ($P<0.05$, Two-way ANOVA; Bonferroni's post hoc test, WT n=11, CK1d$_{T44A}$n=8). Inset: no difference in the paired pulse ratio (PPR) at 50Hz between genotypes ($p>0.05$, Mann Whitney test, WT n=11, CK1d$_{T44A}$n=8). No significant difference between in steady state currents ($p>0.05$, Two-way ANOVA; Bonferroni's post hoc test, WT n=11, CK1d$_{T44A}$n=8) as well as PPR ($p>0.05$, Mann Whitney test, WT n=11, CK1d$_{T44A}$n=8) at 20Hz [g] and 10Hz [h] stimulus trains. Similarly, normalized IPSC plots showing no difference in steady state currents ($p>0.05$, Two-way ANOVA; Bonferroni's post hoc test, WT n=11, CK1d$_{T44A}$n=8) as well as PPR (inset, $p>0.05$, Mann Whitney test, WT n=11, CK1d$_{T44A}$n=8) with [i] 50Hz, [j] 20Hz and [k] 10Hz

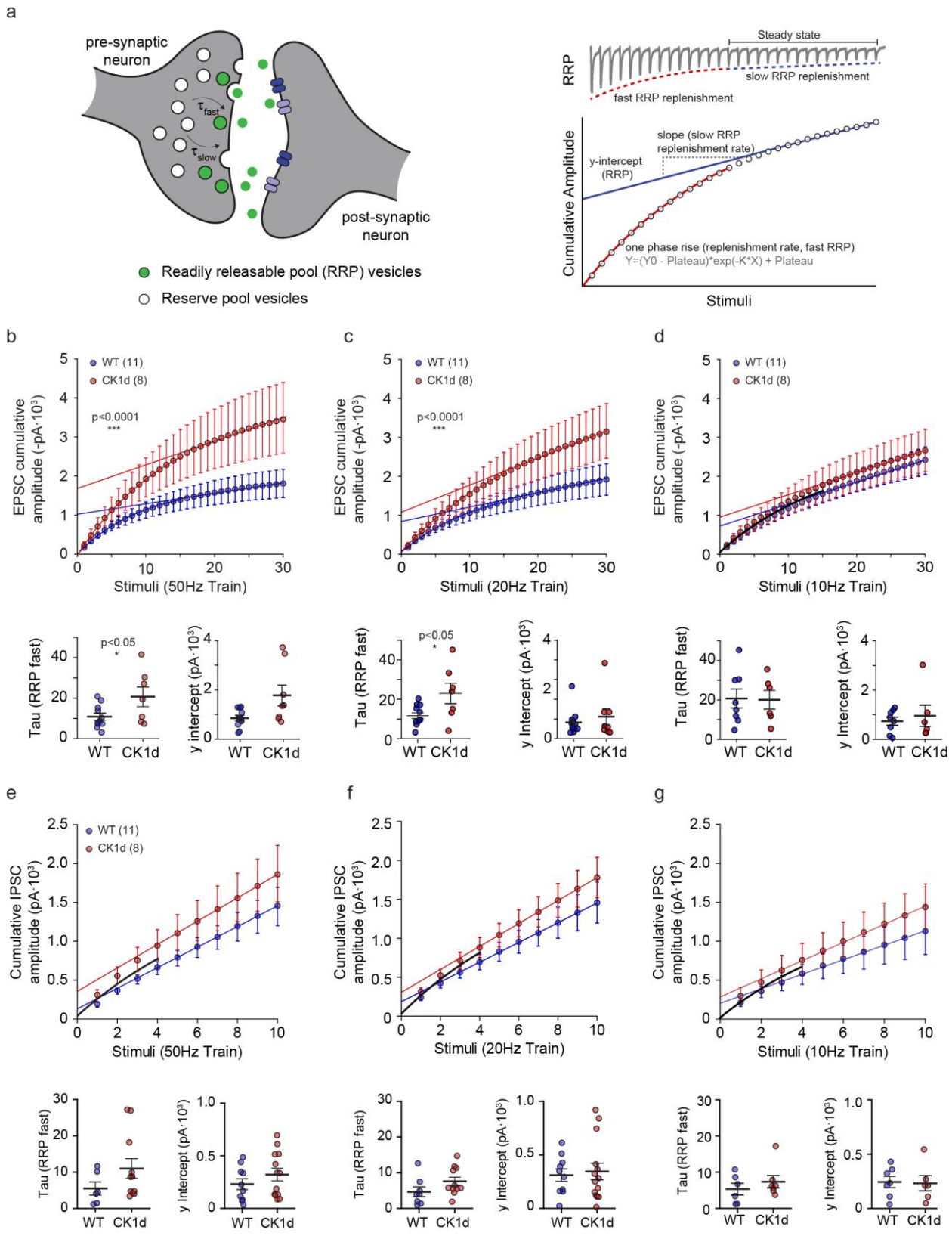

691

Figure 5: Frequency dependent enhancement of fast replenishment of RRP at CK1d$_{T44A}$ excitatory synapses

a] Left: Schematic of a model for RRP replenishment with two distinct components of their kinetics; fast and slow RRP replenishment. Right: Strategy used to analyze replenishment rates of slow and fast components of RRP using cumulative amplitude of post-synaptic response. b] Cumulative EPSC amplitude plot for 50 Hz stim train reveals no difference in the steady state linear regression slope (top, $p>0.05$, ANCOVA, WT n=11, CK1d$_{T44A}$n=8), however initial one phase exponential rise was significantly faster in CK1d$_{T44A}$neurons (top, $p<0.0001$, F test with AIC method, WT n=11, CK1d$_{T44A}$n=8). Insets show no difference in y-intercept values (bottom right, $p=0.08$, Mann Whitney test, WT n=11, CK1d$_{T44A}$n=8) but a significant increase in Tau of fast one phase rise (bottom left, $p<0.05$, Mann Whitney test, WT n=11, CK1d$_{T44A}$n=8) recorded from individual neurons. c] Similarly, significant increase in initial one phase exponential rise in CK1d$_{T44A}$neurons (top, $p<0.0001$, F test with AIC method, WT n=11, CK1d$_{T44A}$n=8) as well as significant increase in Tau of fast one phase rise (bottom left, $p<0.05$, Mann Whitney test, WT n=11, CK1d$_{T44A}$n=8) for EPSCs at 20Hz stimulation. None of the analyzed parameters were found to be significantly different in cumulative EPSC amplitude plot at [d] 10Hz stimulation (top, $p>0.05$, ANCOVA, $p>0.05$, F test with AIC method, WT n=11, CK1d$_{T44A}$ n=8) as well as cumulative IPSC amplitude plots recorded at either [e] 50Hz, [f] 20Hz or [g] 10Hz (top, $p>0.05$, ANCOVA, $p>0.05$, F test with AIC method, WT n=11, CK1d$_{T44A}$ n=8).

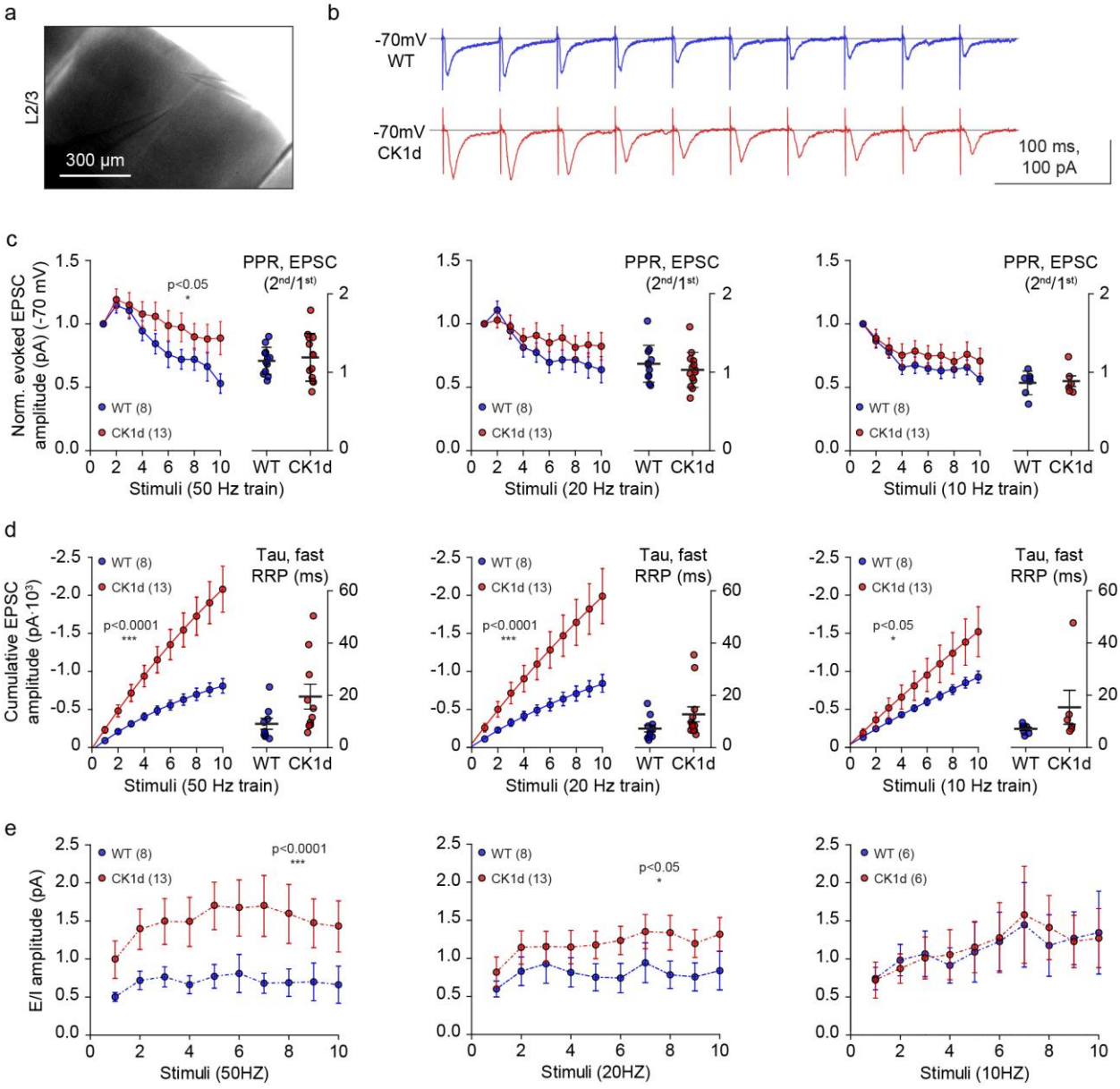

711

Figure 6: Enhanced replenishment of fast component of RRP leads to a net excitatory shift in excitation-inhibition (E/I) balance in CK1d$_{T44A}$

a] Image showing placement of recording and stimulation electrode. b] Representative race showing evoked EPSCs recorded from WT (top, blue) and CK1d$_{T44A}$ (bottom, red) in response to a train of 10 stimuli, at 20Hz. c] Increased steady state EPSC amplitude at 50Hz train of 10 stimuli ($P<0.05$, Two-way ANOVA, WT n=8, CK1d$_{T44A}$n=13) without increase in PPR ($p=0.6$, Mann Whitney test, WT n=8, CK1d$_{T44A}$n=13) at CK1d$_{T44A}$synapses. No difference in steady state EPSC amplitude ($P>0.05$, Two-way ANOVA, WT n=8, CK1d$_{T44A}$n=13) as well as PPR ($p>0.05$, Mann Whitney test, WT n=8, CK1d$_{T44A}$n=13) at [d] 20 Hz and [e] 10 Hz stimulus trains between WT and CK1d$_{T44A}$synapses. Cumulative EPSC amplitude plots show significantly faster kinetics of exponential rise at [f] 50Hz and [g] 20Hz ($p<0.0001$, F-test with AIC method, WT n=8, CK1d$_{T44A}$n=13); as well as in response to [h] 10Hz stimuli ($p<0.05$, F-test with AIC method, WT n=8, CK1d$_{T44A}$n=13). EPSC/IPSC (E/I) ratios recorded from individual neurons reveal a significant shift towards excitation [i] at 50Hz ($p<0.0001$, two-way ANOVA, WT n=8, CK1d$_{T44A}$ n=13) and [j] 20Hz ($p<0.05$, two-way ANOVA, WT n=8, CK1d$_{T44A}$ n=13); in response to trains of 10 stimuli. k] Such a difference in the E/I ratio was not seen at 10Hz ($p>0.05$, two-way ANOVA, WT n=6, CK1d$_{T44A}$n=6).

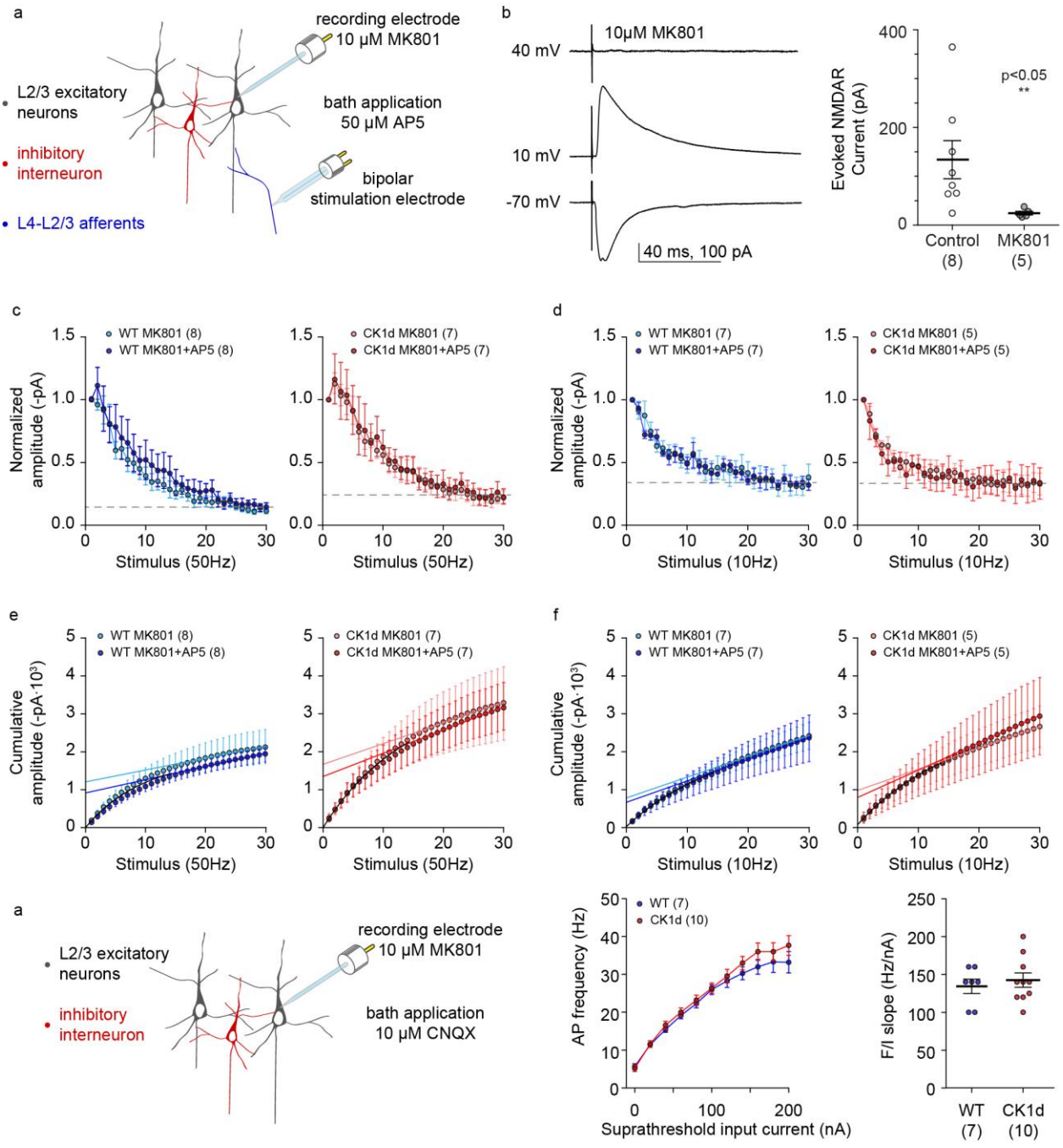

731

Figure 7: Presynaptic NMDARs do not mediate frequency dependent excitatory steady state currents in CK1d$_{T44A}$ synapses

a] Schematic showing strategy for selective blockade of post synaptic (10µM MK801 in patch pipette) as well as presynaptic NMDARs (50µM AP5 bath application). b] Representative traces showing along with quantification of NMDAR currents (V_{Clamp}: 40mV) showing selective blockade of post-synaptic NMDARs with 10µM MK801, yet unaffected AMPAR as well as GABAR mediated E/IPSCs. c] Presynaptic NMDAR blockade with 50µM AP5 had no effect on increased excitatory steady state currents in response to 50Hz stimulation (Left: p>0.05, two-way ANOVA, WT MK801 vs WT MK801+AP5 n=8, Right: p>0.05, two-way ANOVA, CK1d$_{T44A}$MK801 vs CK1d$_{T44A}$MK801+AP5 n=7) as well as d] 10Hz stimulation. e] Initial exponential rise as well as steady state linear regression slopes of cumulative EPSC amplitude plot were not significantly different between WT and CK1d$_{T44A}$at 50Hz (p<0.05, F test with AIC corrections; p>0.05, ANCOVA, WT MK801 vs WT MK801+AP5 n=7, CK1d$_{T44A}$ MK801 vs CK1d$_{T44A}$ MK801+AP5 n=5) as well as f] 10Hz stimulation. g] Schematic showing pharmacological inhibition of post-synaptic NMDARs (10µM MK801 in patch pipette) and AMPARs (20µM CNQX bath application). h] F/I curve (left) demonstrating that inhibition of post-synaptic glutamate receptors normalized input current dependent increase in AP frequency seen in CK1d$_{T44A}$ neurons (p>0.05, two-way ANOVA, WT n=7, CK1d$_{T44A}$ n=10) abolishing differences in F/I curve slopes (right) between genotypes (p>0.05, two-way ANOVA, WT n=7, CK1d$_{T44A}$ n=10).

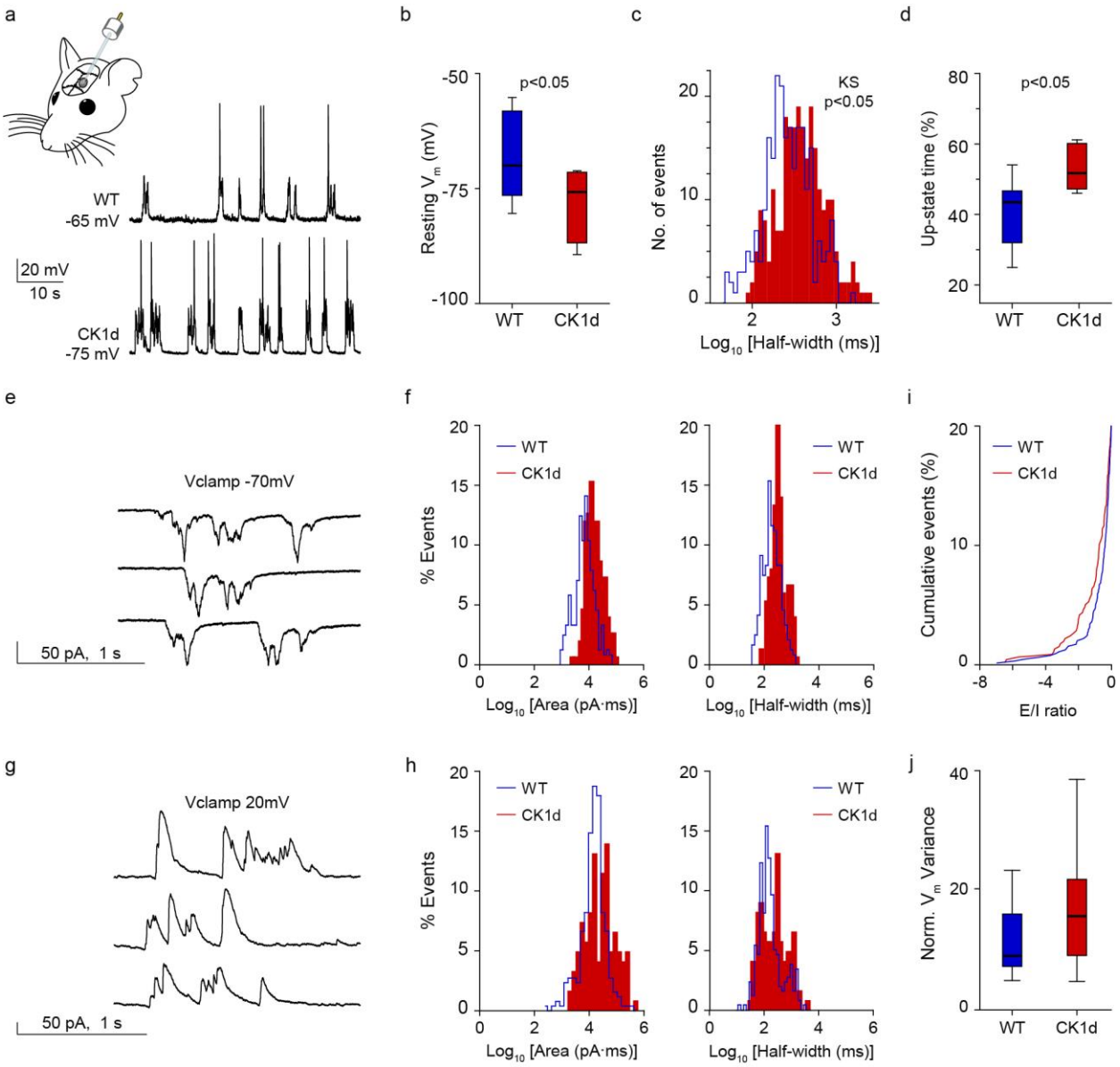

752

Figure 8: Increased up state duration and V_m variance $CK1d_{T44A}$ mice along with net excitatory shift *in vivo*

a] Schematic of *in vivo* whole cell patch clamp experiment as well as representative traces of current clamp recordings of L2/3 pyramidal neurons from WT (top) and $CK1d_{T44A}$ (bottom) mutant mice, showing bistable anesthetized cortical networks (up and down states). b] $CK1d_{T44A}$neurons were significantly hyperpolarized ($p<0.05$, t test, WT n=7, $CK1d_{T44A}$n=5) compared to WT neurons *in vivo*. c] Frequency histograms of up state half-width suggest increased duration of up states in $CK1d_{T44A}$animals ($p<0.05$, 2-sample KS test, WT n=7, $CK1d_{T44A}$n=5). d] $CK1d_{T44A}$ animals also showed an increase in percent time spent in up states ($p<0.05$, t test, WT n=7, $CK1d_{T44A}$n=5). Representative traces showing e] EPSCs and g] IPSCs recorded *in vivo* during an up state event. f] Distribution histograms showing increase in the area and half width of excitatory events ($P<0.05$, 2-sample KS test , WT n=4, $CK1d_{T44A}$n=4), but no difference in the h] area and half width of inhibitory events ($P>0.05$, 2-sample KS test, WT n=4, $CK1d_{T44A}$n=4) in $CK1d_{T44A}$ animals. i] E/I ratio skewed towards excitation in $CK1d_{T44A}$animals ($p<0.05$, 2-sample KS test, WT n=4, $CK1d_{T44A}$n=4). j] Increased membrane potential variance during up states ($p<0.0001$, t test, WT n=4, $CK1d_{T44A}$n=4) in $CK1d_{T44A}$ animals.

References

1. Lipton, R. B. *et al.* Migraine prevalence, disease burden, and the need for preventive therapy. *Neurology* **68**, 343–349 (2007).
2. Stewart, W. F., Ricci, J. A., Chee, E., Morganstein, D. & Lipton, R. Lost productive time and cost due to common pain conditions in the US workforce. *JAMA* **290**, 2443–2454 (2003).
3. Murray, C. J. L. *et al.* Disability-adjusted life years (DALYs) for 291 diseases and injuries in 21 regions, 1990-2010: a systematic analysis for the Global Burden of Disease Study 2010. *Lancet Lond. Engl.* **380**, 2197–2223 (2012).
4. Brennan, K. C. & Pietrobon, D. A Systems Neuroscience Approach to Migraine. *Neuron* **97**, 1004–1021 (2018).
5. Mulleners, W. M. *et al.* Self-reported photophobic symptoms in migraineurs and controls are reliable and predict diagnostic category accurately. *Headache* **41**, 31–39 (2001).
6. Lipton, R. B. *et al.* Cutaneous allodynia in the migraine population. *Ann. Neurol.* **63**, 148–158 (2008).
7. Pietrobon, D. & Moskowitz, M. A. Chaos and commotion in the wake of cortical spreading depression and spreading depolarizations. *Nat. Rev. Neurosci.* **15**, 379–393 (2014).
8. Ambrosini, A. & Schoenen, J. Electrophysiological response patterns of primary sensory cortices in migraine. *J. Headache Pain* **7**, 377–388 (2006).
9. Coppola, G., Pierelli, F. & Schoenen, J. Habituation and migraine. *Neurobiol. Learn. Mem.* **92**, 249–259 (2009).
10. Perlman, R. L. Mouse models of human disease. *Evol. Med. Public Health* **2016**, 170–176 (2016).
11. Pietrobon, D. Cortical spreading depression and familial hemiplegic migraine 2015. *J. Headache Pain* **16**, (2015).

12. Pietrobon, D. Familial hemiplegic migraine. *Neurother. J. Am. Soc. Exp. Neurother.* **4**, 274–284 (2007).

13. Brennan, K. C. *et al.* Casein Kinase Iδ Mutations in Familial Migraine and Advanced Sleep Phase. *Sci. Transl. Med.* **5**, 183ra56-11 (2013).

14. Knippschild, U. *et al.* The casein kinase 1 family: participation in multiple cellular processes in eukaryotes. *Cell. Signal.* **17**, 675–689 (2005).

15. Wolff, S. *et al.* Casein kinase 1 delta (CK1δ) interacts with the SNARE associated protein snapin. *FEBS Lett.* **580**, 6477–6484 (2006).

16. Greer, Y. E., Gao, B., Yang, Y., Nussenzweig, A. & Rubin, J. S. Lack of Casein Kinase 1 Delta Promotes Genomic Instability - The Accumulation of DNA Damage and Down-Regulation of Checkpoint Kinase 1. *PLOS ONE* **12**, e0170903 (2017).

17. Etchegaray, J.-P. *et al.* Casein Kinase 1 Delta Regulates the Pace of the Mammalian Circadian Clock. *Mol. Cell. Biol.* **29**, 3853–3866 (2009).

18. Sawant-Pokam, P. M., Suryavanshi, P., Mendez, J. M., Dudek, F. E. & Brennan, K. C. Mechanisms of Neuronal Silencing After Cortical Spreading Depression. *Cereb. Cortex N. Y. N 1991* **27**, 1311–1325 (2017).

19. Zhang, Z., Matos, S. C., Jego, S., Adamantidis, A. & Séguéla, P. Norepinephrine Drives Persistent Activity in Prefrontal Cortex via Synergistic α1 and α2 Adrenoceptors. *PLOS ONE* **8**, e66122 (2013).

20. Sheets, P. L. *et al.* Corticospinal-specific HCN expression in mouse motor cortex: Ih-dependent synaptic integration as a candidate microcircuit mechanism involved in motor control. *J. Neurophysiol.* **106**, 2216–2231 (2011).

816 21. Petersen, C. C. H. & Sakmann, B. The Excitatory Neuronal Network of Rat Layer 4
817 Barrel Cortex. *J. Neurosci.* **20**, 7579–7586 (2000).
818 22. Varela, J. A., Song, S., Turrigiano, G. G. & Nelson, S. B. Differential Depression at
819 Excitatory and Inhibitory Synapses in Visual Cortex. *J. Neurosci.* **19**, 4293–4304 (1999).
820 23. Guo, J. *et al.* A Three-Pool Model Dissecting Readily Releasable Pool Replenishment at
821 the Calyx of Held. *Sci. Rep.* **5**, (2015).
822 24. Kaeser, P. S. & Regehr, W. G. The readily releasable pool of synaptic vesicles. *Curr.*
823 *Opin. Neurobiol.* **43**, 63–70 (2017).
824 25. Farrant, M. & Nusser, Z. Variations on an inhibitory theme: phasic and tonic activation of
825 $GABA_A$ receptors. *Nat. Rev. Neurosci.* **6**, 215–229 (2005).
826 26. Chergui, K., Svenningsson, P. & Greengard, P. Physiological role for casein kinase 1 in
827 glutamatergic synaptic transmission. *J. Neurosci. Off. J. Soc. Neurosci.* **25**, 6601–6609 (2005).
828 27. Kase, D. & Imoto, K. The Role of HCN Channels on Membrane Excitability in the
829 Nervous System. *Journal of Signal Transduction* (2012). doi:10.1155/2012/619747
830 28. Cheetham, C. E. J. & Fox, K. Presynaptic Development at L4 to L2/3 Excitatory
831 Synapses Follows Different Time Courses in Visual and Somatosensory Cortex. *J. Neurosci.*
832 **30**, 12566–12571 (2010).
833 29. Lefort, S. & Petersen, C. C. H. Layer-Dependent Short-Term Synaptic Plasticity Between
834 Excitatory Neurons in the C2 Barrel Column of Mouse Primary Somatosensory Cortex.
835 *Cereb. Cortex* **27**, 3869–3878 (2017).
836 30. Fioravante, D. & Regehr, W. G. Short-term forms of presynaptic plasticity. *Curr. Opin.*
837 *Neurobiol.* **21**, 269–274 (2011).

838 31. Abrahamsson, T. *et al.* Differential Regulation of Evoked and Spontaneous Release by
839 Presynaptic NMDA Receptors. *Neuron* **96**, 839-855.e5 (2017).
840 32. Luo, H., Hasegawa, K., Liu, M. & Song, W.-J. Comparison of the Upper Marginal
841 Neurons of Cortical Layer 2 with Layer 2/3 Pyramidal Neurons in Mouse Temporal Cortex.
842 *Front. Neuroanat.* **11**, (2017).
843 33. Douglas, R. J., Koch, C., Mahowald, M., Martin, K. A. C. & Suarez, H. H. Recurrent
844 Excitation in Neocortical Circuits. *Science* **269**, 981–985 (1995).
845 34. Wilson, C. Up and down states. *Sch. J.* **3**, 1410 (2008).
846 35. Gerkin, R. C., Clem, R. L., Shruti, S., Kass, R. E. & Barth, A. L. Cortical Up State
847 Activity Is Enhanced After Seizures: A Quantitative Analysis. *J. Clin. Neurophysiol. Off.*
848 *Publ. Am. Electroencephalogr. Soc.* **27**, 425–432 (2010).
849 36. Bragin, A., Benassi, S. K. & Engel, J. Patterns of the Up-Down State in normal and
850 epileptic mice. *Neuroscience* **225**, 76–87 (2012).
851 37. Anderson, J. S., Lampl, I., Gillespie, D. C. & Ferster, D. The contribution of noise to
852 contrast invariance of orientation tuning in cat visual cortex. *Science* **290**, 1968–1972 (2000).
853 38. Theriot, J. J., Toga, A. W., Prakash, N., Ju, Y. S. & Brennan, K. C. Cortical sensory
854 plasticity in a model of migraine with aura. *J. Neurosci. Off. J. Soc. Neurosci.* **32**, 15252–
855 15261 (2012).
856 39. Tottene, A. *et al.* Enhanced Excitatory Transmission at Cortical Synapses as the Basis for
857 Facilitated Spreading Depression in CaV2.1 Knockin Migraine Mice. *Neuron* **61**, 762–773
858 (2009).

40. Tottene, A. *et al.* Familial hemiplegic migraine mutations increase Ca(2+) influx through single human CaV2.1 channels and decrease maximal CaV2.1 current density in neurons. *Proc. Natl. Acad. Sci. U. S. A.* **99**, 13284–13289 (2002).

41. Capuani, C. *et al.* Defective glutamate and K+ clearance by cortical astrocytes in familial hemiplegic migraine type 2. *EMBO Mol. Med.* e201505944 (2016). doi:10.15252/emmm.201505944

42. Dilekoz, E. *et al.* Migraine Mutations Impair Hippocampal Learning Despite Enhanced Long-Term Potentiation. *J. Neurosci.* **35**, 3397–3402 (2015).

43. Xu, Y. *et al.* Functional consequences of a CKIdelta mutation causing familial advanced sleep phase syndrome. *Nature* **434**, 640–644 (2005).

44. Coppola, G. *et al.* Interictal abnormalities of gamma band activity in visual evoked responses in migraine: an indication of thalamocortical dysrhythmia? *Cephalalgia Int. J. Headache* **27**, 1360–1367 (2007).

45. Lampl, I. & Katz, Y. Neuronal adaptation in the somatosensory system of rodents. *Neuroscience* **343**, 66–76 (2017).

46. Wark, B., Lundstrom, B. N. & Fairhall, A. Sensory adaptation. *Curr. Opin. Neurobiol.* **17**, 423–429 (2007).

47. Heiss, J. E., Katz, Y., Ganmor, E. & Lampl, I. Shift in the balance between excitation and inhibition during sensory adaptation of S1 neurons. *J. Neurosci. Off. J. Soc. Neurosci.* **28**, 13320–13330 (2008).

48. Isaacson, J. S. & Scanziani, M. How Inhibition Shapes Cortical Activity. *Neuron* **72**, 231–243 (2011).

881 49. Higley, M. J. & Contreras, D. Balanced excitation and inhibition determine spike timing
882 during frequency adaptation. *J. Neurosci. Off. J. Soc. Neurosci.* **26**, 448–457 (2006).
883 50. Hsu, S.-F., Augustine, G. J. & Jackson, M. B. Adaptation of Ca2+-Triggered Exocytosis
884 in Presynaptic Terminals. *Neuron* **17**, 501–512 (1996).
885 51. Regehr, W. G. Short-Term Presynaptic Plasticity. *Cold Spring Harb. Perspect. Biol.* **4**,
886 a005702 (2012).
887 52. Lipstein, N. *et al.* Dynamic Control of Synaptic Vesicle Replenishment and Short-Term
888 Plasticity by Ca2+-Calmodulin-Munc13-1 Signaling. *Neuron* **79**, 82–96 (2013).
889 53. Bui, L. & Glavinović, M. I. Is replenishment of the readily releasable pool associated
890 with vesicular movement? *Cogn. Neurodyn.* **8**, 99–110 (2014).
891 54. Martin, T. F. J. Tuning exocytosis for speed: fast and slow modes. *Biochim. Biophys.*
892 *Acta BBA - Mol. Cell Res.* **1641**, 157–165 (2003).
893 55. Inchauspe, C. G. *et al.* Presynaptic CaV2.1 calcium channels carrying familial hemiplegic
894 migraine mutation R192Q allow faster recovery from synaptic depression in mouse calyx of
895 Held. *J. Neurophysiol.* **108**, 2967–2976 (2012).
896 56. Alabi, A. A. & Tsien, R. W. Synaptic Vesicle Pools and Dynamics. *Cold Spring Harb.*
897 *Perspect. Biol.* **4**, (2012).
898 57. Yamasaki, T., Kawasaki, H. & Nishina, H. Diverse Roles of JNK and MKK Pathways in
899 the Brain. *Journal of Signal Transduction* (2012). doi:10.1155/2012/459265
900 58. Fourcaudot, E. *et al.* cAMP/PKA signaling and RIM1α mediate presynaptic LTP in the
901 lateral amygdala. *Proc. Natl. Acad. Sci.* **105**, 15130–15135 (2008).

902 59. Bidoret, C., Ayon, A., Barbour, B. & Casado, M. Presynaptic NR2A-containing NMDA
903 receptors implement a high-pass filter synaptic plasticity rule. *Proc. Natl. Acad. Sci.*
904 pnas.0904284106 (2009). doi:10.1073/pnas.0904284106
905 60. Banerjee, A., Larsen, R. S., Philpot, B. D. & Paulsen, O. Roles of Presynaptic NMDA
906 Receptors in Neurotransmission and Plasticity. *Trends Neurosci.* **39**, 26–39 (2016).
907 61. Brasier, D. J. & Feldman, D. E. Synapse-Specific Expression of Functional Presynaptic
908 NMDA Receptors in Rat Somatosensory Cortex. *J. Neurosci.* **28**, 2199–2211 (2008).
909 62. Yang, J., Woodhall, G. L. & Jones, R. S. G. Tonic Facilitation of Glutamate Release by
910 Presynaptic NR2B-Containing NMDA Receptors Is Increased in the Entorhinal Cortex of
911 Chronically Epileptic Rats. *J. Neurosci.* **26**, 406–410 (2006).
912 63. Larsen, R. S. *et al.* Synapse-specific control of experience-dependent plasticity by
913 presynaptic NMDA receptors. *Neuron* **83**, 879–893 (2014).
914 64. Zhou, N. *et al.* Regenerative glutamate release by presynaptic NMDA receptors
915 contributes to spreading depression. *J. Cereb. Blood Flow Metab. Off. J. Int. Soc. Cereb.*
916 *Blood Flow Metab.* **33**, 1582–1594 (2013).
917 65. Ma, C., Su, L., Seven, A. B., Xu, Y. & Rizo, J. Reconstitution of the vital functions of
918 Munc18 and Munc13 in neurotransmitter release. *Science* **339**, 421–425 (2013).
919 66. Yang, X. *et al.* Syntaxin opening by the MUN domain underlies the function of Munc13
920 in synaptic-vesicle priming. *Nat. Struct. Mol. Biol.* **22**, 547–554 (2015).
921 67. A phosphatidylinositol 4,5-bisphosphate-sensitive casein kinase I alpha associates with
922 synaptic vesicles and phosphorylates a subset of vesicle proteins. *J. Cell Biol.* **130**, 711–724
923 (1995).

924 68. Zhang, N. *et al.* Phosphorylation of Synaptic Vesicle Protein 2A at Thr84 by Casein
925 Kinase 1 Family Kinases Controls the Specific Retrieval of Synaptotagmin-1. *J. Neurosci.* **35**,
926 2492–2507 (2015).
927 69. Pyle, R. A., Schivell, A. E., Hidaka, H. & Bajjalieh, S. M. Phosphorylation of synaptic
928 vesicle protein 2 modulates binding to synaptotagmin. *J. Biol. Chem.* **275**, 17195–17200
929 (2000).
930 70. Buxton, P. *et al.* Identification and characterization of Snapin as a ubiquitously expressed
931 SNARE-binding protein that interacts with SNAP23 in non-neuronal cells. *Biochem. J.* **375**,
932 433–440 (2003).
933 71. Murray, M. M., Lewkowicz, D. J., Amedi, A. & Wallace, M. T. Multisensory Processes:
934 A Balancing Act across the Lifespan. *Trends Neurosci.* **39**, 567–579 (2016).
935 72. Haider, B. & McCormick, D. A. Rapid neocortical dynamics: cellular and network
936 mechanisms. *Neuron* **62**, 171–189 (2009).
937 73. Zagha, E. & McCormick, D. A. Neural control of brain state. *Curr. Opin. Neurobiol.* **29**,
938 178–186 (2014).
939 74. Bartram, J. *et al.* Cortical Up states induce the selective weakening of subthreshold
940 synaptic inputs. *Nat. Commun.* **8**, 665 (2017).
941 75. Petersen, C. C. H., Hahn, T. T. G., Mehta, M., Grinvald, A. & Sakmann, B. Interaction of
942 sensory responses with spontaneous depolarization in layer 2/3 barrel cortex. *Proc. Natl.*
943 *Acad. Sci.* **100**, 13638–13643 (2003).
944 76. Hodkinson, D. J. *et al.* Increased Amplitude of Thalamocortical Low-Frequency
945 Oscillations in Patients with Migraine. *J. Neurosci.* **36**, 8026–8036 (2016).

946 77. Meis, S., Endres, T., Munsch, T. & Lessmann, V. Presynaptic Regulation of Tonic
947 Inhibition by Neuromodulatory Transmitters in the Basal Amygdala. *Mol. Neurobiol.* **55**,
948 8509–8521 (2018).
949 78. Glykys, J. & Mody, I. The main source of ambient GABA responsible for tonic inhibition
950 in the mouse hippocampus. *J. Physiol.* **582**, 1163–1178 (2007).
951 79. Song, I. *et al.* Different transporter systems regulate extracellular GABA from vesicular
952 and non-vesicular sources. *Front. Cell. Neurosci.* **7**, 23 (2013).
953 80. Richerson, G. B. & Wu, Y. Dynamic Equilibrium of Neurotransmitter Transporters: Not
954 Just for Reuptake Anymore. *J. Neurophysiol.* **90**, 1363–1374 (2003).
955 81. Wu, Y., Wang, W. & Richerson, G. B. GABA Transaminase Inhibition Induces
956 Spontaneous and Enhances Depolarization-Evoked GABA Efflux via Reversal of the GABA
957 Transporter. *J. Neurosci.* **21**, 2630–2639 (2001).
958 82. Wu, Y., Wang, W., Díez-Sampedro, A. & Richerson, G. B. Nonvesicular inhibitory
959 neurotransmission via reversal of the GABA transporter GAT-1. *Neuron* **56**, 851–865 (2007).
960 83. Medrihan, L., Ferrea, E., Greco, B., Baldelli, P. & Benfenati, F. Asynchronous GABA
961 Release Is a Key Determinant of Tonic Inhibition and Controls Neuronal Excitability: A
962 Study in the Synapsin II−/− Mouse. *Cereb. Cortex* **25**, 3356–3368 (2015).
963 84. Lebas, A. *et al.* Severe Attacks of Familial Hemiplegic Migraine, Childhood Epilepsy
964 and ATP1A2 Mutation. *Cephalalgia* **28**, 774–777 (2008).
965